Supplement of Atmos. Meas. Tech., 18, 7153–7176, 2025 https://doi.org/10.5194/amt-18-7153-2025-supplement © Author(s) 2025. CC BY 4.0 License.





# Supplement of

# A helicopter-based mass balance approach for quantifying methane emissions from industrial activities, applied for coal mine ventilation shafts in Poland

Eric Förster et al.

Correspondence to: Eric Förster (eric.foerster@dlr.de) and Heidi Huntrieser (heidi.huntrieser@dlr.de)

The copyright of individual parts of the supplement might differ from the article licence.

# S1 Meteorological situation and flight overview

During the first field experiment in June 2022, two major frontal systems with embedded deep convection passed over the USCB region, causing variable wind conditions in strength and direction and partly cloudy conditions. Ahead of the frontal system, prevailing winds were blowing from the SW which advected haze, pollution, and once even Saharan dust to the region. After the frontal passage, NW winds brought cleaner air to the region. A summary of all MTG-Poland flights, with flight number, take-off and landing time and targets are listed in Table S1.

Table S1. Summary of the HELiPOD mission flights during the METHANE-To-Go-Poland field campaign in June and October 2022.

Date	Flight	Time (LT)	Duration	Target	Additional source
June					
2022-06-13 <b>a</b> /Mon	F01	10:35-10:45	0h 10 min	HELiPOD Training	
2022-06-13 <b>b</b> /Mon	F02	10:50-11:40	0h 50 min	Test Flight	
2022-06-14a /Tue	F03	09:30-11:40	2h 10 min	Knurów-Szczygłowice IV	
2022-06-14 <b>b</b> /Tue	F04	14:20-17:30	3h 10 min	Knurów-Szczygłowice IV	Drainage station D1
2022-06-15 /Wed	F05	10:15-13:35	2h 20 min	Knurów-Szczygłowice IV	
2022-06-16 /Thu	F06	09:55-12:35	2h 40 min	Knurów-Szczygłowice IV	Drainage station D1
2022-06-18a /Sat	F07	09:05-11:50	2h 45 min	Knurów-Szczygłowice IV	
2022-06-18 <b>b</b> /Sat	F08	14:10-16:40	2h 30 min	Brzeszcze-Andrzej IX	
2022-06-20 /Mon	F09	08:05-11:20	3h 15 min	Pniówek V	
2022-06-21 /Tue	F10	17:10-20:20	3h 10 min	Brzeszcze-Andrzej IX	Drainage station D2
2022-06-22 <b>a</b> /Wed	F11	08:30-09:00	0h 30 min	Technical Flight	
2022-06-22 <b>b</b> /Wed	F12	10:30-13:50	3h 20 min	Brzeszcze-Andrzej IX	
2022-06-23 /Thu	F13	08:05-11:25	3h 20 min	Pniówek V	
October					
2022-10-10 /Mon	F01	12:30-15:30	3h 00 min	Pniówek V	
2022-10-11 /Tue	F02	16:30-18:15	1h 45 min	Brzeszcze-Andrzej IX	
2022-10-12 /Wed	F03	11:10-14:20	3h 10 min	Pniówek V	
2022-10-13 /Thu	F04	13:40-16:20	2h 40 min	Brzeszcze-Andrzej IX	
2022-10-14 /Fri	F05	10:10-13:20	3h 10 min	Pniówek V	
2022-10-16 /Sun	F06	12:10-15:10	3h 00 min	Agnieszka-Powietrzny V	Shaft Erbreich-Powietrzny I and drainage station D4
2022-10-17 <b>a</b> /Mon	F07	10:00-13:15	3h 30 min	Agnieszka-Powietrzny V	Shaft Erbreich-Powietrzny I and drainage station D4
2022-10-17 <b>b</b> /Mon	F08	14:30-15:40	1h 10 min	First controlled CH <sub>4</sub> release	
2022-10-18 /Tue	F09	11:25-12:25	1h 00 min	Second controlled CH <sub>4</sub> release	

The weather conditions in October 2022 were different from the conditions during the campaign in June. In autumn, high pressure situations were more frequent with several pronounced inversion layers. Such stable layers have a major influence on the distribution of CH<sub>4</sub> emissions from the ventilation shafts and act as a cap hindering dispersion in the vertical direction.

# **S2** Calibrations

Fig. S1 and Table S2 show a summary of all CH<sub>4</sub> calibrations for the Picarro G2401-m, hereafter simply named as Picarro, and the Licor LI-7700, hereafter simply named as Licor, performed during the 2022 June field campaign. Calibrations during the 2022 October campaign were similar, albeit with lower frequency. Three different Air Liquide standards (NOAA corrected) for CH<sub>4</sub> were used (high: 2689 ppb, middle: 1845 ppb and low: 1625 ppb). We note, that the ppb and ppm notation which is widely used in the trace gas community refers hereafter to mole fractions. The concentrations of the Air Liquide standards were determined before and after the campaign using the Picarro and two NOAA standards with an accuracy of ~2 ppb.

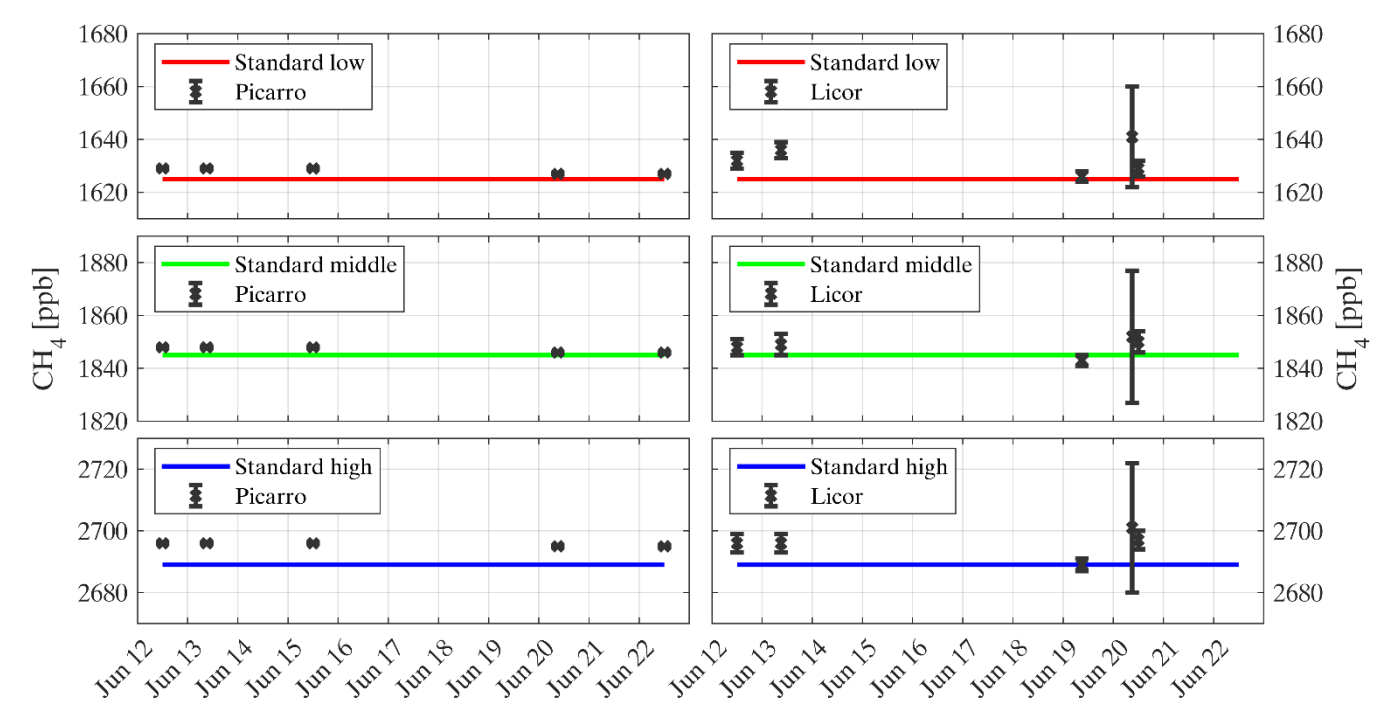


**Figure S1.** Summary of the Picarro G2401-m (left) and Licor LI-7700 (right) calibrations during the MTG-Poland field campaign in June 2022 for NOAA-corrected Air Liquide gas standards with high, middle, and low CH<sub>4</sub> concentrations. The mean standard deviation is 0.15 ppb for the Picarro and 3 ppb for the Licor. The large standard deviation on 20 June 2022 is related to a contamination of the Licor mirror. After the mirror cleaning on the same day, the standard deviation decreased.

**Table S2.** Summary of the Picarro G2401-m and Licor LI-7700 calibrations during the June field campaign. The averaging time was 1.5 minutes. The RSSI (Residual Signal Strength Indicator) is approx. 80 % in most cases. During Flight F09 on 20 June, the mirror was contaminated and the calibration #1 was done with post-flight RSSI of 40 % and repeated after the mirror cleaning (calibration #2). The delta  $(\Delta)$  states the absolute difference between measured and certified mixing ratios.

			Picarro [ppl	b]					Licor [pp	b]		
	Low		Medium		High		Low		Medium	1	High	
Certified	1625	Δ	1845	Δ	2689	Δ	1625	Δ	1845	Δ	2689	Δ
12 June	1629 ± 0.15	4	1848 ± 0.15	3	2696 ± 0.15	7	1632 ± 3	7	1848 ± 3	3	2696 ± 3	7
13 June	1629 ± 0.15	4	1848 ± 0.15	3	2696 ± 0.15	7	1636 ± 3	11	1849 ± 4	4	2696 ± 3	7
15 June	1629 ± 0.15	4	1848 ± 0.15	3	2696 ± 0.15	7						
19June							1626 ± 2	1	1843 ± 2	-2	2689 ± 2	0
20 June #1	1627 ± 0.15	3	1846 ± 0.15	1	2695 ± 0.15	6	1641 ± 19	16	1852 ± 25	7	2701 ± 21	12
20 June #2							1629 ± 3	4	1850 ± 4	5	2697 ± 3	8
22 June	1627 ± 0.15	3	1846 ± 0.15	1	2695 ± 0.15	6						

The on-site calibrations of the Picarro in Bielsko-Biała during the two campaigns in June and October 2022 did not show any significant trends, deviations or outliers compared to the laboratory calibrations which were performed against NOAA primary standards. The deviation of the Picarro measurements to the NOAA standards is small. Nevertheless, we corrected the measurement data with Eq. S1:

$$CH_4 \text{ (corrected)} = 0.99747 * CH_4 \text{ dry [ppm]} + 0.00151 \text{ [ppm]}$$
 (S1)

The factors of Eq. S1 were determined with a linear fit of the measured Picarro CH<sub>4</sub> concentrations against the concentrations given on the gas standard certificates.

The Licor was serviced and recalibrated by the manufacturer before the June campaign. We calibrated the Licor and Picarro in Bielsko-Biała against the three Air Liquide standards during the June and October 2022 campaign every second to third day and found no trends or outliers (except for the outlier mentioned above). In general, the deviations are small (only a few ppb) and in the order of the standard deviation. Therefore, no corrections were applied.

#### S3 Calculation of the CH<sub>4</sub> mass balance: An example

The processing and calculation procedure are exemplarily shown for three mass balance experiments (MBE) of Flight 07 during the autumn campaign, on 17 October 2022, with take-off at 10:00 LT (local time). The top view and cross section of the MBEs are shown in the main document in Fig. 3 to Fig. 5.

# Calculation steps

In the following section, detailed steps of the systematic CH<sub>4</sub> mass flux calculation, based on Eq. 3 in the main document (which is given again in Eq. S2), are described exemplarily for MBE 2 (H6 to C6) in Fig. 5 in the main document. The index i indicates a pointwise mass flux calculation which means, that the flux is calculated for every 2 Hz (Picarro) or 40 Hz (Licor) measurement separately.

$$F_i = [\Delta C]_i \cdot \frac{M_{CH_4} \cdot p_i}{R T_i} U_{\perp,i} \cdot W_i \cdot H_i$$
 (S2)

 $F_i$  = discrete mass flux for a pointwise measurement [kg s<sup>-1</sup>]

 $[\Delta C]_i$  pointwise CH<sub>4</sub> enhancement above the background concentration [mol mol<sup>-1</sup>], see Eq. S3

 $M = \text{molar mass of CH}_4 \text{ [kg mol}^{-1}\text{]}$ 

 $p_i$  = air pressure [Pa]

 $R = \text{universal gas constant } [\text{J mol}^{-1} \text{ K}^{-1}]$ 

 $T_i$  = temperature [K]

 $U_{\perp,i}$  = perpendicular component of the wind speed to the performed MBE [m s<sup>-1</sup>]

 $W_i$  = horizontal extension of  $\Delta C_i$  [m], equal to the distance between two pointwise measurements

 $H_i$  = vertical extension of  $\Delta C_i$  [m]

Step 1 to 5 describe the calculation of  $\Delta C_i$ ,  $U_{\perp,i}$ ,  $W_i$ ,  $H_i$  and  $F_i$ .

# Step 1: CH<sub>4</sub> enhancement and background

The CH<sub>4</sub> enhancement is calculated by subtracting the CH<sub>4</sub> background concentration from the measured CH<sub>4</sub> value (Eq. S3):

$$[\Delta C]_i = [C]_i - [C]_{ba} \tag{S3}$$

 $C = CH_4 [ppm]$ 

The CH<sub>4</sub> background [C]<sub>bg</sub> is determined by interpolating between 10-second averages of both transect edges (following Pühl et al., 2024). If both averages differ more than 50 ppb it is assumed that there is a plume present at either one of both edges and only the smaller mean value is used as background value. This method was successful for most of the transects, notwithstanding that the background concentration may change by an order of magnitude within a typical transect length up to 10 km. Methane plumes are then identified by  $\Delta$ CH<sub>4</sub> > 3 $\sigma$ , with  $\sigma$  being the mean of two root-mean-square errors (RMSE) of both 10-second time periods used for CH<sub>4</sub> background calculation of the transect edges. This procedure covers the variability of the background concentration and therefore we do not assess the uncertainty of the background separately. Usually, 3 $\sigma$  is smaller than 10 ppb. In a few cases, plumes of nearby sources (e.g. shafts and drainage stations) could not be separated with the default threshold of 3 $\sigma$  and then a higher threshold is manually defined to separate the peaks. However, this approach may lead to a slight underestimation of mass fluxes due to the cut-off of the plume edges. Upwind curtains were not used for the determination of background concentrations, but only for cross-checking the values of the transect edge method and to identify potential additional emission sources.

# Step 2: CH<sub>4</sub> plume selection

Figure S2 shows identified CH<sub>4</sub> plumes using Step 1. The main CH<sub>4</sub> plume (present up to transect TS 8) probed by the *HELiPOD*, ranged from enhancements of 2 ppm at ground levels (obtained by mobile ground-based measurements: GB) to 0.2 ppm at TS 8. At TS 9, the plume is not visible, hence the top of the plume is estimated to be located between TS 8 and TS 9 (as indicated in the centre figure). Mobile ground-based measurements were performed close to the airborne *HELiPOD* measurements, as indicated by the co-located ground-based plume in Fig. S3.

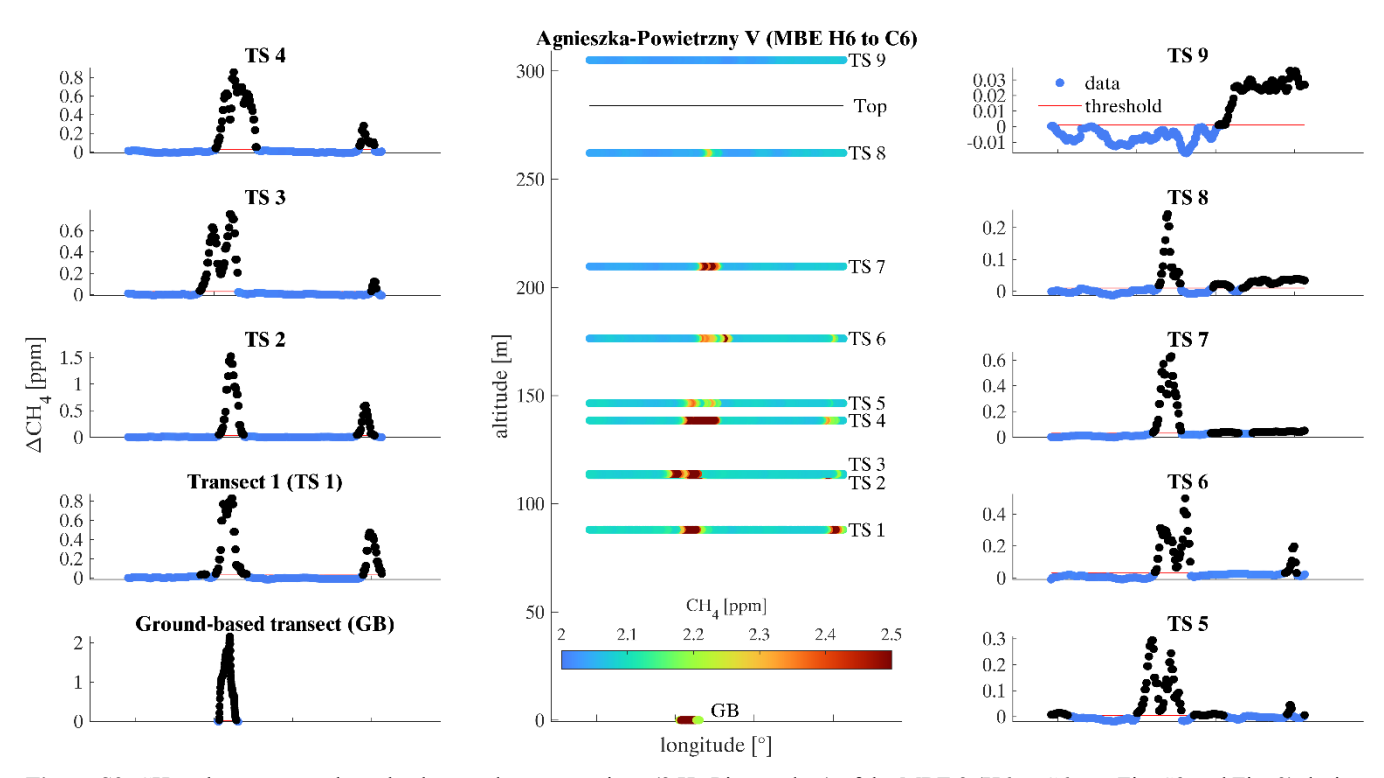
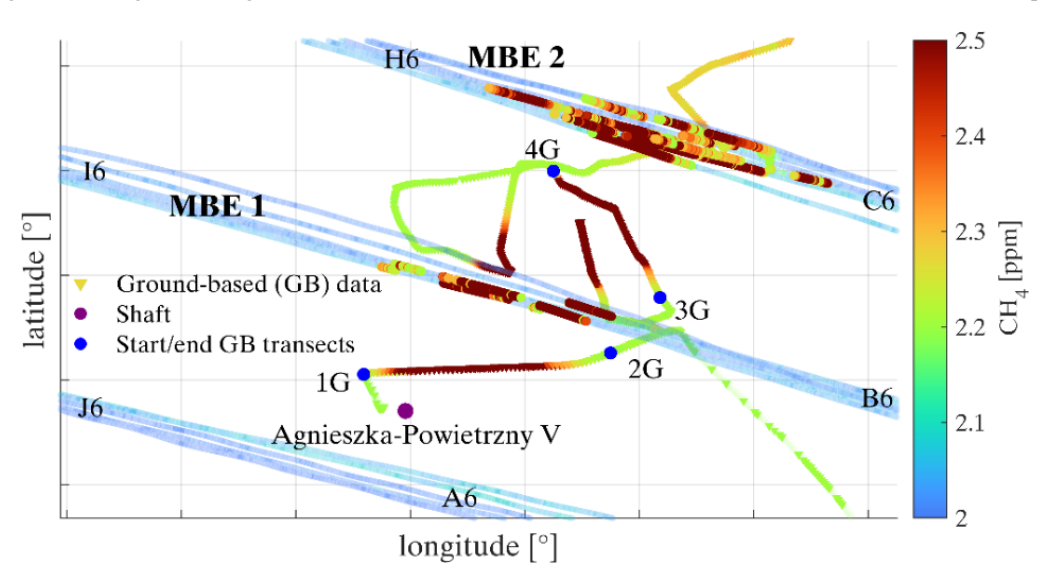
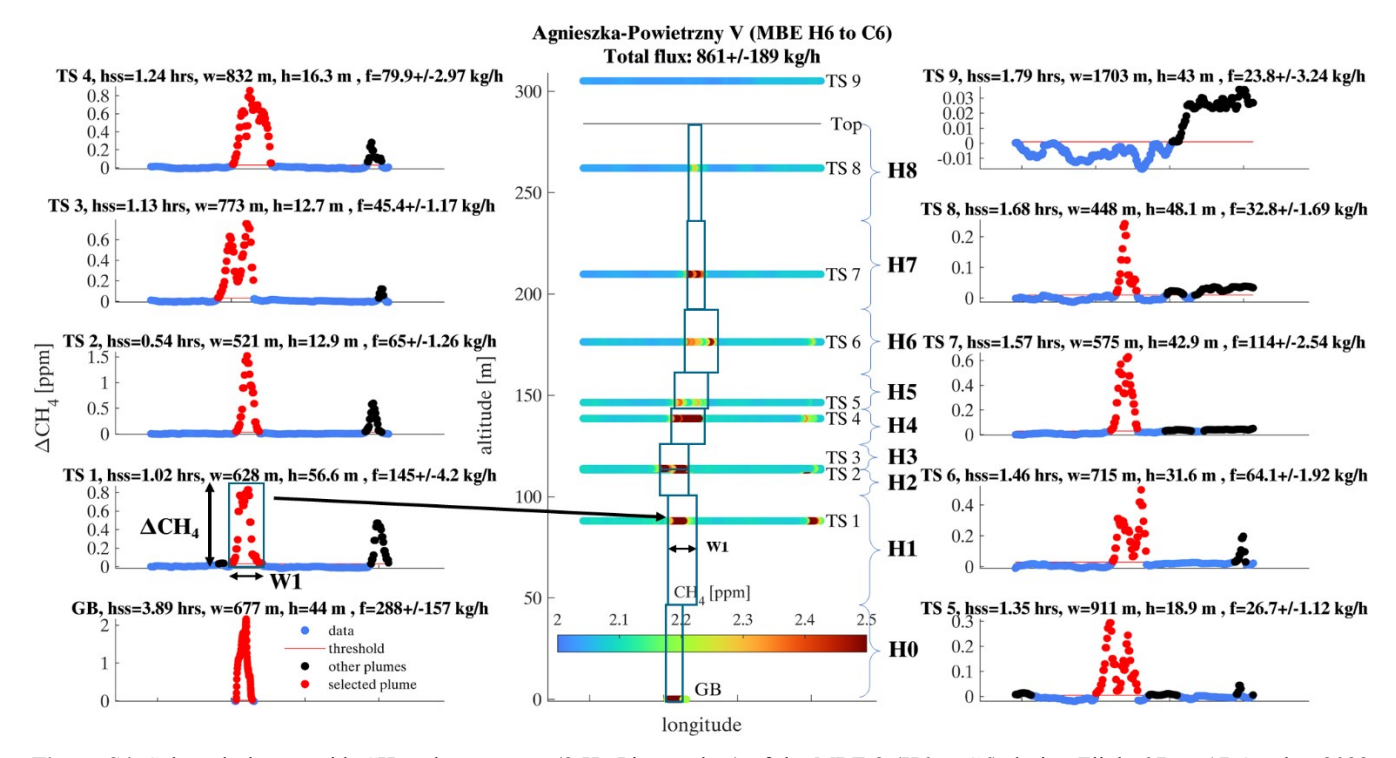


Figure S2. CH4 enhancements above background concentrations (2 Hz Picarro data) of the MBE 2 (H6 to C6, see Fig. S3 and Fig. 3) during Flight 07 on 17 October 2022 (take-off 10:00 LT), probing the shaft Agnieszka-Powietrzny V (left black plume). The red thin line indicates the plume identification threshold, which is  $3\sigma$  of the two 10-second time periods (left and right of the selected plume) used for CH4 background calculation (see Step 1). The second plume, on the right side of the transect was attributed to a nearby drainage station and can also be used for a mass flux estimate. The centre panel shows the cross section of the airborne and ground-based transects, colour-coded with CH4 mixing ratios. The given average altitude for each transect is calculated from the measurements of the identified plumes.



**Figure S3.** Top view of the *HELiPOD* transects of MBE 1 (I6 to B6) and MBE 2 (H6 to C6) with additional ground-based measurements (irregular pathways) during Flight 07 on 17 October 2022 probing the shaft Agnieszka-Powietrzny V. The GB transect between the points 3G and 4G is used for MBE 1 and MBE 2. The GB transect 1G to 2G is too close to the shaft and not representative for MBE 1.

From the identified plumes, the ones which most likely originate from the targeted shaft are selected for the mass flux calculation. The selection for MBE 2 of Flight 07 on 17 October 2022 is obvious: the large peak on the left side of every transect belongs to the shaft Agnieszka-Powietrzny V (Fig. S4). The second peak on the right side belongs to the nearby drainage station and this plume can also be used for a mass flux estimate.



**Figure S4.** Selected plumes with CH<sub>4</sub> enhancements (2 Hz Picarro data) of the MBE 2 (H6 to C6) during Flight 07 on 17 October 2022 (take-off 10:00 LT). Same as Fig. S2, however here the red plumes have been selected for the calculation of the CH<sub>4</sub> mass flux originating from the shaft Agnieszka-Powietrzny V. Black coloured enhancements are originating from other sources, like a drainage station in this specific case. The boxes in the centre panel indicate the plume width (**W**) and height (**H**), where each box reach halfway down to the next lower and halfway up to the next higher transect. Through these rectangles (layers), the mass flux is estimated. Abbreviations: TS - transect, hss - hours since take-off, w – plume width, h – plume height, f - flux of transect based on selected plumes (red). The total CH<sub>4</sub> flux calculated for MBE 2 from the 2 Hz Picarro data, including ground-based (GB) measurements, is 861 kg h<sup>-1</sup> ± 189 kg h<sup>-1</sup>.

# Step 3: Perpendicular component U⊥ of the wind speed

The perpendicular component of the wind speed  $U_{\perp}$  is calculated based on the measured wind speed, wind direction and heading of the *HELiPOD* (Eq. S4).

$$U_{\perp,i} = \left| sin\left( (HH_i - DD_i) \cdot \frac{\pi}{180} \right) \right| \cdot FF_i$$
 (S4)

 $HH_i$  = pointwise heading of HELiPOD [°]

 $DD_i$  = pointwise wind direction of HELiPOD [°]

 $FF_i$  = pointwise wind speed of HELiPOD [m s<sup>-1</sup>]

Comparisons between *HELiPOD* and mobile ground-based wind measurements during the release experiment at the Bielsko-Biała airfield (Fig. S5 and Fig. S6) indicated that the measured wind direction on the ground has a very high variability (Fig. S6). In contrast, the HELiPOD measurements, carried out in very low altitude (3 m to 30 m), show stable wind directions around 220°. We observed this high variability in wind direction in many cases for the ground-based transects, which partly led, if used for the mass flux calculations, even to negative mass fluxes for the ground layer. Therefore, the mean wind speed and direction of the lowest *HELiPOD* transect was instead combined with the ground-based CH<sub>4</sub> measurements for the mass flux calculation at ground level, obtaining better mass flux estimates.

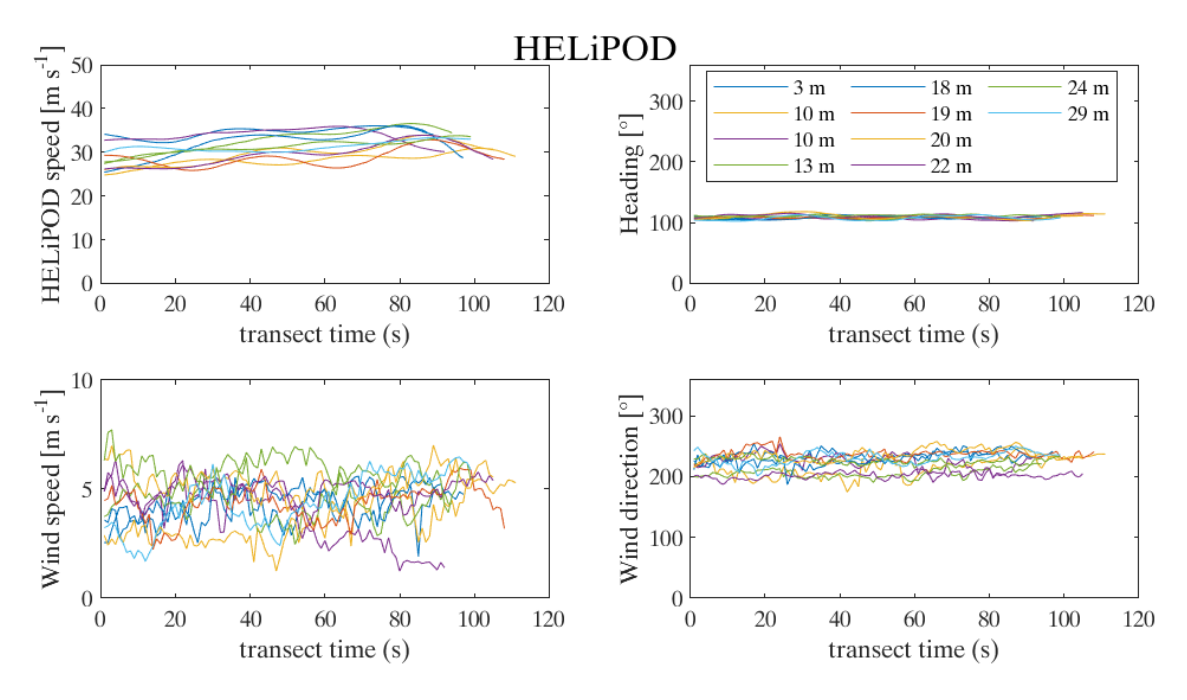


Figure S5. HELiPOD speed (top left), heading (top right), wind speed (bottom left) and wind direction (bottom right) for 10 transects in different altitudes during the first release experiment (Flight 8, 17 October 2022) at the Bielsko-Biała airfield.

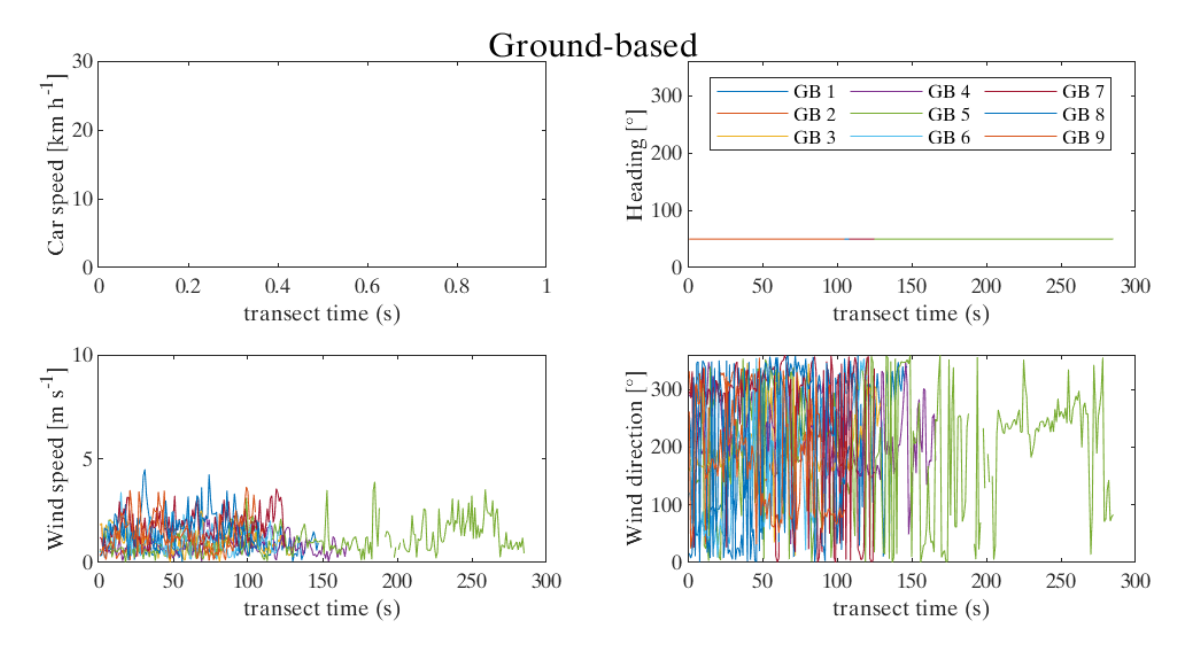


Figure S6. Like Fig. S5, just for nine ground-based (GB) transects performed by car. For the car speed no data was available.

### Step 4: Plume height $H_i$ and width $W_i$

The top of the plume is an important parameter for an accurate mass flux quantification. Usually, we measure up to altitudes were no CH<sub>4</sub> enhancement is present in order to estimate the plume top. In cases where we do not reach the top of the plume with our measurements, we assume that the next inversion layer or the PBL acts as a cap for the investigated CH<sub>4</sub> plumes. To estimate the PBL height, vertical profiles were flown before and after each target probing. Figure S7 shows vertical profiles of (i) the potential temperature  $\theta$  and its vertical gradient  $d\theta$   $dz^{-1}$ , (ii) the CH<sub>4</sub> and H<sub>2</sub>O mixing ratio and (iii) the wind speed FF and direction DD. At the PBL height strong vertical changes of  $\theta$ , trace gas mixing ratios, FF and DD occur which indicates the boundary between air masses with different properties and dynamical behaviour. On 17 October at ~10:30 LT, the PBL is located at ~750 m. A second weaker inversion layer might be present at ~500 m (change of wind direction and larger  $d\theta$   $dz^{-1}$ ). From Fig. 5 (main document) it becomes clear that the plume of the shaft Agnieszka-Powietrzny V does not reach the PBL or

the inversion layer during MBE 1 and 2. Especially close to the source, where the plume still disperses in the vertical, it is important to probe transects above the plume to estimate its maximal vertical extent (since here it is still not fully mixed up to the PBL). The vertical plume extent is one of the parameters needed for the mass flux calculations.

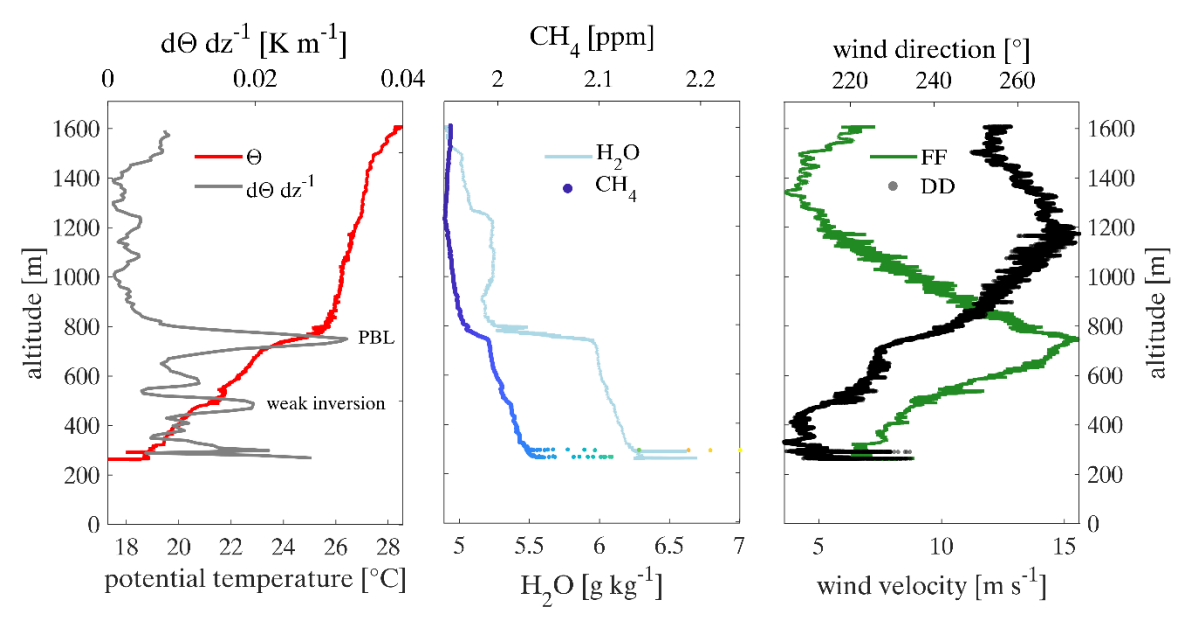


Figure S7. Vertical descending profile on the way to the shaft Agnieszka-Powietrzny V on 17 October from 10:20 until 10:28 LT. Shown are the potential temperature and its gradient (left), the CH<sub>4</sub> and H<sub>2</sub>O mixing ratios (middle) and the wind speed and direction (right). These profiles indicate that the PBL is located at  $\sim$ 750 m and a second weaker inversion layer at  $\sim$ 500 m.

The height  $H_i$  of a plume transect j is estimated to be a layer around the transect which reaches halfway down to the mean altitude of the plume at the next higher transect  $((A_i - A_{i-1})/2)$  and halfway up to the mean altitude of the plume at the next higher transect  $((A_{i+1}-A_i)/2)$ . If no ground-based data is included, the plume layer of the lowest transect TS 1 is estimated to reach down to the ground. If the highest transect still shows enhancements, which can be attributed to the targeted source, the layer is estimated to reach halfway down to the mean altitude of the plume at the next lower transect and all the way up to the estimated PBL height. If a plume does not reach to the highest flown transect, we estimate the plume top to be halfway up to the mean altitude of the next higher transect. The mean altitudes A are calculated from the measurements within the plume transect (not from the complete transect).

$$H = \frac{A_j - A_{j-1}}{2} + \frac{A_{j+1} - A_j}{2} = \frac{A_{j+1} - A_{j-1}}{2}$$
 (S5)

A = mean altitude of a selected plume j [m]

The plume width  $W_i$  of a pointwise measurement is calculated based on the velocity of the HELiPOD and the measurement frequency:

$$W_i = v_i \cdot \Delta t \tag{S6}$$

 $v_i$  = pointwise speed of *HELIPOD* during measurement [m s<sup>-1</sup>]

 $\Delta t$  = measurement frequency [s]

# Step 5: CH<sub>4</sub> mass flux calculation

The mass flux is now calculated by summing up the pointwise estimated mass fluxes  $F_i$  (every 2 Hz, 40 Hz, 100 Hz, respectively) to gain a mass flux  $F_j$  per plume. Usually j=1, as for the example above. If more plumes belong to the targeted source, the mass fluxes  $F_j$  are summed up to gain a mass flux  $F_k$  per transect. Finally, the total mass flux F is the sum of  $F_k$  for each selected transect (Eq. 4 in the main document). From all flown transects which cover mostly up to 2.5 hours, we select

those which are temporally close to each other (probed within  $\sim 1\,$  h) to receive approximately constant meteorological conditions. In that way, we can derive two estimates from one MBE, one at the beginning and one at the end of a flight (see e.g. Table S7).

In the example of MBE 2 during Flight 07 on 17 October 2022, the total CH<sub>4</sub> flux from the 2 Hz Picarro data, including ground-based (GB) measurements, is  $861 \text{ kg h}^{-1} \pm 189 \text{ kg h}^{-1}$ . The estimation of the mass flux uncertainty is addressed in Sect. S5. The CH<sub>4</sub> mass flux for MBE 1 and MBE 3 are calculated accordingly (Table S3).

Table S3. Calculated CH4 flux rates of the shaft Agnieszka-Powietrzny V for three MBEs at different distances (D) to the emission source, probed during Flight 07 on 17 October 2022 (take-off 10:00 LT), calculated separately with data from the Picarro and the Licor instrument with original data resolution (2 Hz and 40 Hz, respectively) and upsampled 100 Hz data. Uncertainties are calculated using Gaussian error propagation (see Sect. S5). Abbreviations: D – distance of MBE to shaft, R – measurement frequency of data, GB – ground-based transects included or not (yes/no), FF – wind speed, DD – wind direction, Ø - average for all plumes of the wall, σ - root-mean-square error, A TS1 – altitude of lowest transect, Top – plume height, IL height of inversion layer. The bold values are used to calculate the final mass flux estimate for the shaft Agnieszka-Powietrzny V during Flight 07.

												H	ELiPOD	In-m	ine data	relative
MDE	D		R	GB	FF [n	n s <sup>-1</sup> ]	DD	) [°]	A TS1	Top	IL	flux	flux unc.	flux	flux unc.	deviation
MBE	[m]	Instrument	[Hz]	added	Ø	σ	Ø	σ		[m]			[kg	; h <sup>-1</sup> ]		[%]
	660	Picarro	2	no	6.3	1.5	213	8.1	109	190	490	761	302	1011	202	-25
	660	Picarro	100	no	6.2	1.3	213	7.9	109	191	490	757	322	1011	202	-25
	660	Licor	40	no	6.2	1.3	213	7.9	106	193	490	746	329	1011	202	-26
MBE 1	660	Licor	100	no	6.2	1.3	213	7.9	107	192	490	743	345	1011	202	-27
(I6-B6)	660	Picarro	2	yes	6.2	1.4	212	8.1	108	193	490	900	249	1011	202	-11
	660	Picarro	100	yes	5.9	1.2	212	8.3	108	193	490	898	263	1011	202	-11
	660	Licor	40	yes	5.9	1.2	212	8.3	106	193	490	877	259	1011	202	-13
	660	Licor	100	yes	5.9	1.2	212	8.3	106	192	490	877	271	1011	202	-13
	1570	Picarro	2	no	5.8	1.5	211	11.0	88	284	490	710	148	1011	202	-29
	1570	Picarro	100	no	5.8	1.4	211	11.0	88	284	490	706	171	1011	202	-29
	1570	Licor	40	no	5.8	1.4	211	11.0	91	284	490	704	204	1011	202	-29
MBE 2	1570	Licor	100	no	5.8	1.4	211	11.0	90	284	490	708	215	1011	202	-29
(H6-C6)	1570	Picarro	2	yes	5.8	1.5	211	11.0	88	284	490	861	189	1011	202	-13
	1570	Picarro	100	yes	5.8	1.4	211	11.0	88	284	490	855	207	1011	202	-14
	1570	Licor	40	yes	5.8	1.4	211	11.0	91	284	490	858	233	1011	202	-14
	1570	Licor	100	yes	5.8	1.4	211	11.0	90	284	490	857	241	1011	202	-14
	3550	Picarro	2	no	5.7	1.7	210	10.0	129	490	490	398	75	1011	202	-61
MBE 3	3550	Picarro	100	no	5.4	1.4	210	10.0	129	490	490	404	89	1011	202	-60
(G6-D6)	3550	Licor	40	no	5.4	1.4	210	10.0	129	490	490	390	162	1011	202	-61
	3550	Licor	100	no	5.4	1.4	210	10.0	129	490	490	390	166	1011	202	-61
	Mean	(bold values)			6.0	1.5	212	9.6	98	239	490	881	221	1011	202	-14

In general, mass fluxes are calculated for all curtains downwind of a targeted shaft, if plumes could clearly be linked to the emissions from a given shaft. For comparison, mass fluxes are calculated separately with data from the Picarro and the Licor instrument with original data resolution (2 Hz and 40 Hz, respectively), as well as for upsampled 100 Hz data. Furthermore, if mobile ground-based measurements can reasonably be included, i.e. a full plume crossing is ensured and they are co-located to the *HELiPOD* measurements in time (< 1 h) and space (mean distance < 500 m), mass fluxes are calculated with and without including ground-based data.

Table S3 shows the mass flux estimates for Flight 07 on 17 October 2022 based on the two different CH<sub>4</sub> instruments and for three MBEs with respective wind conditions and plume properties. The Picarro and Licor measurements mostly yield the same mass flux estimates within a maximum deviation of 23 kg h<sup>-1</sup> (MBE 1 with added GB data), corresponding to ~3 % relative deviation. Furthermore, data up-sampling to 100 Hz produces similar results for both instruments (see Sect. S6.1 for a detailed comparison between both instruments).

Mass flux rates differ from MBE to MBE and also depend on whether ground-based data is included. However, MBE 1 and 2 agree well within their uncertainty ranges, whether ground-based data is included (Picarro: 900 kg h<sup>-1</sup>  $\pm$  249 kg h<sup>-1</sup> and 861 kg h<sup>-1</sup>  $\pm$  189 kg h<sup>-1</sup>, respectively) or excluded (Picarro: 761 kg h<sup>-1</sup>  $\pm$  302 kg h<sup>-1</sup> and 710 kg h<sup>-1</sup>  $\pm$  148 kg h<sup>-1</sup>, respectively). During MBE 3, the plumes of the shaft Agnieszka-Powietrzny V and shaft Erbreich-Powietrzny I began to mix, resulting in a broad

plume with two distinct peaks. We tried to separate the plume peak of the shaft Agnieszka-Powietrzny V, but the complete emissions could not be selected following Step 2. This is the reason why the mass fluxes of MBE 3 are lower.

The final mean mass flux of the shaft Agnieszka-Powietrzny V for Flight 07 on 17 October 2022 is calculated from 2 Hz Picarro mass flux estimates for MBE 1 and MBE 2 by including ground-based transects, but neglecting MBE 3. We only use Picarro measurements because a comparison to the Licor instrument revealed an excellent agreement ( $R^2 = 0.99$ ) with the Picarro having generally lower mass flux uncertainties (median 8 % lower). Hence, the total mean mass flux of the shaft Agnieszka-Powietrzny V for Flight 07 is 881 kg h<sup>-1</sup>  $\pm$  221 kg h<sup>-1</sup>. Other flights are analysed in the same way. For all mean values per flight and targeted source given in Table 4 in the main document, 2 Hz Picarro is used and only MBEs with ground-based measurements are included if they are available. MBEs are neglected for the calculation of the mean values if it cannot be ruled out that the mass flux is influenced by emissions of other sources.

#### S4 Estimation of mass flux uncertainties

Uncertainties are calculated using Gaussian error propagation (Eq. S7), with F calculated according to Eq. S2, as described in the main document. Here the separate  $\sigma$  are described.

$$F_{i_{unc}} = \sqrt{\sum_{i} \left(\frac{\partial F_{i}(x_{i})}{\partial x_{i}} \cdot \sigma\right)^{2}}$$
 (S7)

For  $x = \Delta CH_4$ 

σ CH<sub>4</sub> Picarro (2 Hz): 0.00216 ppm precision

σ CH<sub>4</sub> Licor (40 Hz): 0.020 ppm precision, accuracy: 1 % of reading

The precision of the Licor is estimated from the given value stated by the manufacturer (0.005 ppm at 10 Hz).  $\sigma$   $\Delta$ CH<sub>4</sub> is either the instrumental uncertainty (considered two times due to the background subtraction:  $\sqrt{\sigma}$  CH<sub>4</sub><sup>2</sup> +  $\sigma$  CH<sub>4</sub><sup>2</sup> ) or the RMSE  $\sigma$  of the two 10-second time periods of the transect edges (used for determination of the background concentration), whatever value is larger. The uncertainty of the calculated background concentration is covered by the plume selection through  $\Delta$ CH<sub>4</sub> > 3 $\sigma$ , where 3 $\sigma$  is in the range of several ppb. This magnitude corresponds also to uncertainties of mean background concentrations calculated by Cambaliza et al., (2014).

# For x = wind

 $\sigma_{UL}$  is calculated via Gaussian error propagation from Eq. S4 using Eq. S7 with  $F = U_L$ , and

 $\sigma_{HH}$  = RMSE of heading HH during plume transect

 $\sigma_{DD} = 3$ ° for the pointwise *HELiPOD* measurements

 $\sigma_{FF} = 0.1 \text{ m s}^{-1}$  for the pointwise *HELiPOD* measurements

The technology of determining the wind vector (vector difference between airspeed vector and groundspeed vector, see Pätzold et al., 2023) and methods of calibration are equal to the state-of-the-art research aircraft; thus, the uncertainty of the wind measurement is comparable (see, e.g. Lampert et al., 2020). Compared to the wind measurement of the DLR Cessna Grand Caravan 208B (Fiehn et al., 2020), thoroughly described in Mallaun et al. (2015), for the HELiPOD the approach of calibration manoeuvres is applied, utilizing wind calibration pattern (wind square) flown roughly at each second flight of the campaign.

For the ground-based measurements the mean wind speed and direction from the plume of the lowest transect are taken, hence  $\sigma_{DD} = \text{RMSE}$  of DD from the plume of the lowest transect

 $\sigma_{FF}$  = RMSE of FF from the plume of the lowest transect

#### For x = p

 $\sigma_p$  is either the instrumental uncertainty (5 Pa) or the RMSE during plume transect, whatever is larger.

# For x = T

 $\sigma_T$  is either the instrumental uncertainty (0.1 K) or the RMSE during plume transect, whatever is larger.

# For x = W

 $\sigma_L = \sigma_v \cdot \Delta t$ , with  $\sigma_v = \text{RMSE}$  of *HELiPODs* velocity v during the plume transect, assuming that  $\sigma \Delta t = 0$ .

#### Uncertainty for the height of the plume

For the height of individual layers around the transect, no uncertainty is specified. Instead, we calculate mass flux uncertainties introduced by the estimated top of the plume and the plume extrapolation to the ground (only if no ground-based data is available).

 $F_{unc\_top}$  is the mass flux uncertainty introduced by the uncertainty of the estimated top of the plume. This uncertainty is estimated to be half the distance to the next higher transect with no CH<sub>4</sub> enhancement (if applicable). If the highest probed transect still shows CH<sub>4</sub> enhancements, the uncertainty of the top of the plume is estimated to be half the distance until the inversion layer/PBL. From this distance  $F_{unc\_top}$  is calculated.

 $F_{unc\_bottom}$  is the uncertainty introduced by extrapolating the plume to the ground if no ground-based data is available. The uncertainty of the height of the lower plume limit is then estimated to be half the distance from the lowest probed transect to the ground. From this distance  $F_{unc\_bottom}$  is calculated. If ground-based data is available,  $F_{unc\_bottom} = 0$ .

# Total mass flux uncertainty

Similar to the total mass flux given by Eq. 4 in the main document, the pointwise uncertainties  $F_{i_{unc}}$ , plumewise uncertainties  $F_{j_{unc}}$  and transectwise uncertainties  $F_{k_{unc}}$  are summed up to obtain a mass flux uncertainty  $F_{unc\_flux}$ . The uncertainties  $F_{unc\_top}$  and  $F_{unc\_bottom}$ , given as mass fluxes resulting from the uncertain plume height, are added to  $F_{unc\_flux}$  to obtain the total mass flux uncertainty  $F_{unc}$ , following Eq. S7. We use this more conservative uncertainty approach due to the closer probing to emission sources where the plume is not yet well mixed in the PBL.

$$F_{unc} = F_{unc\ flux} + F_{unc\ top} + F_{unc\ bottom}$$
 (S7)

#### Example for MBE 2, Flight 7 on 17 October 2022

The uncertainty from the ground-based transect is 157 kg h<sup>-1</sup> and generally larger due to the application of RMSE of DD and FF from the lowest *HELiPOD* transect for  $\sigma_{DD}$  and  $\sigma_{FF}$ . The uncertainty from the single transects TS 1 to TS 8 is ~17 kg h<sup>-1</sup>. The top of the plume is estimated to be between TS 8 and 9 (since TS 9 has no enhancements). The respective uncertainty is 21.5 m (half distance from TS 8 to TS 9), resulting in a mass flux uncertainty of 15 kg h<sup>-1</sup>. Hence, the total mass flux uncertainty is 157 kg h<sup>-1</sup> + 17 kg h<sup>-1</sup> + 15 kg h<sup>-1</sup> = 189 kg h<sup>-1</sup>.

The CH<sub>4</sub> mass flux uncertainty is driven by different parameters, as discussed above. Figure S8 shows the different contributions for the Picarro and Licor measurements. For Picarro, 76 % of the total uncertainty is determined by the

uncertainty of the top of the plume and the wind speed. Another 22 % is driven by the uncertainty of the plume base. Due to the high precision of the Picarro, its contribution is negligible. In contrast, the lower precision of the Licor contributes to 13 % to the total mass flux uncertainty.

Plume probing under certain conditions can lead to a reduced uncertainty of the CH<sub>4</sub> mass flux. Taking the Picarro uncertainty range of 5 % to 115 % from the 51 MBEs that were calculated as a basis (neglecting the mobile ground-based measurements), Table S4 introduces several possibilities for reduction of uncertainty.

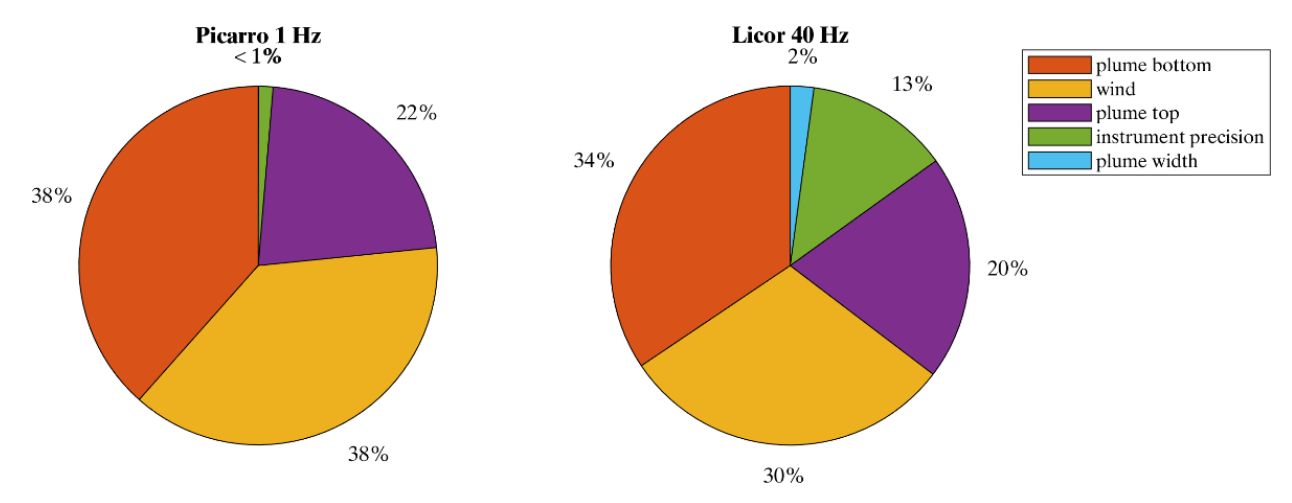


**Figure S8.** Contribution of single parameters to the total mass flux uncertainty considering the uncertainties of the plume base, the wind, the plume top, the instrument precision and the plume width. Mass flux uncertainties are taken from all conducted 51 MBEs and averaged with the geometric average.

Table S4. Improvement of the relative mass flux uncertainty under certain conditions for selected parameters and their combination.

			Uncerta	inty [%]
Case	Parameter(s)	Number of MBEs	min	max
	No specific selection	51	5	115
1	Distance of MBE to source > 2000 m	16	5	51
2	Altitude of lowest transect <= 100 m	23	5	51
3	Wind speed $> 3.5 \text{ m s}^{-1}$	39	5	48
4	Number of transects > 4	28	5	50
5	Altitude of highest transect > 300 m	20	5	51
6	Case 4 and 5	15	5	50
7	Case 3, 4 and 5	11	13	44
8	Case 2, 3, 4 and 5	4	13	24
9	Mobile ground-based data included	15	11	41

Improvement of uncertainties below 51 % can be achieved by either probing the plume at a distance of more than 2000 m, or probing the lowest transect below 100 m, or probing at wind speed of more than 3.5 m s<sup>-1</sup>, or flying more than four transects per MBE, or probing a plume with the highest altitude above 300 m. The latter indicates that the plume top is accurately identified. Combinations of these conditions can further reduce the uncertainty below 24 %

# S5 Further sensitivity studies

# S5.1 Comparing Picarro- and Licor-based mass flux estimates

As described in Sect. 2.2 in the main document, the two instruments Picarro and Licor are based on different measurement techniques (CRDS and open path infrared absorption, respectively) and have different temporal resolutions (2 Hz and 40 Hz, respectively). They were deployed to complement each other in respect of precision and temporal resolution. Despite their technical differences, the calculated mass fluxes of both instruments are in excellent agreement with a R<sup>2</sup> of 0.99 (Fig. S9a).

The original 2 Hz and 40 Hz CH<sub>4</sub> measurements were upsampled to 100 Hz to fit the frequency of the meteorological data. Here, the agreement of mass fluxes based on original and up sampled measurements is also excellent (Fig. S9b).

In addition, the mass flux uncertainties between the instruments agree (Fig. S10a), but with Picarro tending to have smaller uncertainties (median 8 % smaller). This is especially the case when probing farther away from the source (Fig. S10b), leading to differences of up to ~50 % in the relative uncertainty. Here the Licor measurements are noisier compared to the Picarro measurements due to smaller CH<sub>4</sub> enhancements and a decreased RSSI at the end of the flight caused by mirror contamination. Although measurements of both instruments result in comparable mass flux estimates and uncertainties, we recommend deploying both on the *HELiPOD* in future field experiments, since they have complementary strengths: The fast Licor is able to capture sharp CH<sub>4</sub> peaks close to the emission source, which supports the source attribution, whereas the more precise Picarro is better suited to measure small enhancements farther away from the source. Furthermore, the operation of two CH<sub>4</sub> instruments on the *HELiPOD* reduces the risk for data gaps.

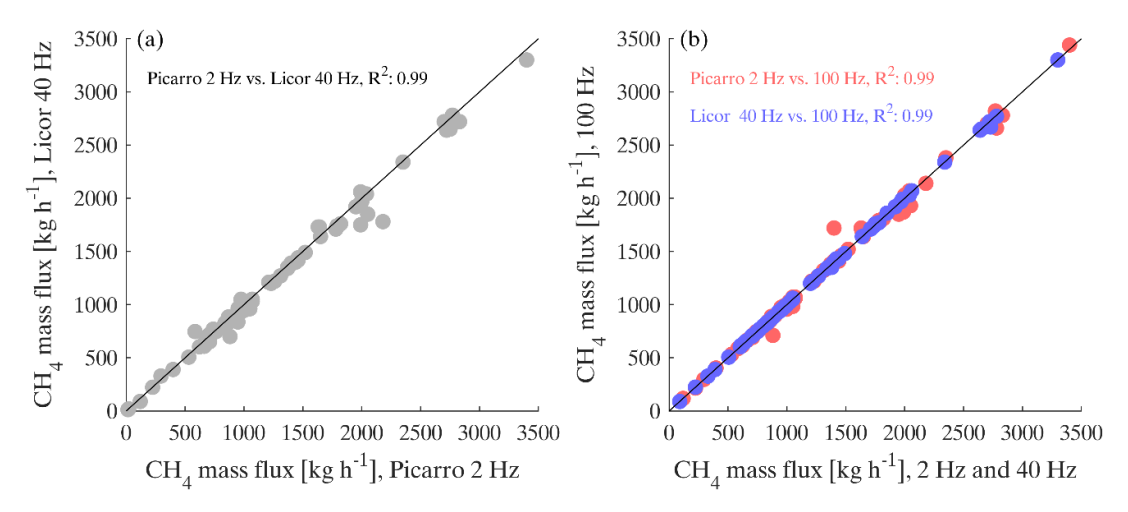


**Figure S9.** Comparison of mass flux estimates based on CH<sub>4</sub> measurements of two different instruments for all 59 mass balance experiments. **(a)** 2 Hz Picarro versus 40 Hz Licor measurements. **(b)** 2 Hz Picarro and 40 Hz Licor measurements versus upsampled 100 Hz data.

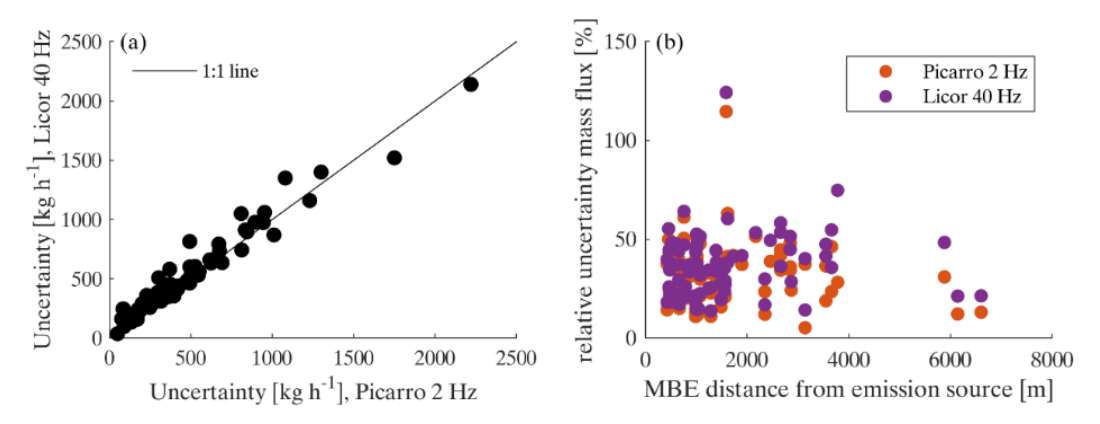


**Figure S10.** Comparison of mass flux uncertainties based on CH<sub>4</sub> measurements of two different instruments for all 59 MBEs. (a) 2 Hz Picarro versus 40 Hz Licor measurements. (b) Relative uncertainty in dependency of the MBE distance from the emission source for 2 Hz Picarro and 40 Hz Licor measurements.

# S5.2 Density of probing

MBEs in different distances to the emission source (Fig. 11a, b) show a weak relationship with the mass flux uncertainties and the deviation to bottom-up data. The higher uncertainties occur again during low wind speed and when very close to the source. In general, the optimal horizontal probing distance strongly depends on the source strength, the meteorological conditions (e.g. wind, atmospheric stability), the temporal resolution of the instrument, the velocity of the measurement platform, as well as characteristics of the surrounding environment (i.e. vegetation, topography, remoteness). Measurements should not be taken too far away from the source because of plume dispersion and the greater possibility of mixing with other nearby CH<sub>4</sub> sources.

By contrast, when flying too close to a source, the horizontal/vertical extension of the plume might be too narrow (especially at higher wind speed), which leads to a poor coverage with only a few measurement points. From our experience with the *HELiPOD*, we recommend to fly MBEs not closer than 500 m to 1000 m and not farther away than 5000 m downwind of the CH<sub>4</sub> source, if the estimated source strength is >500 kg h<sup>-1</sup>. We conclude that there is no specific optimal distance, but a preferred distance range of ~500 m to 5000 m in which MBEs with the *HELiPOD* should be conducted. This is analogous to the US EPA OTM33A (United States Environmental Protection Agency, Other Test Method 33A) ground based plume method that has a range of 20 m to 200 m downwind of sources small in spatial extent (Edie et al., 2020).

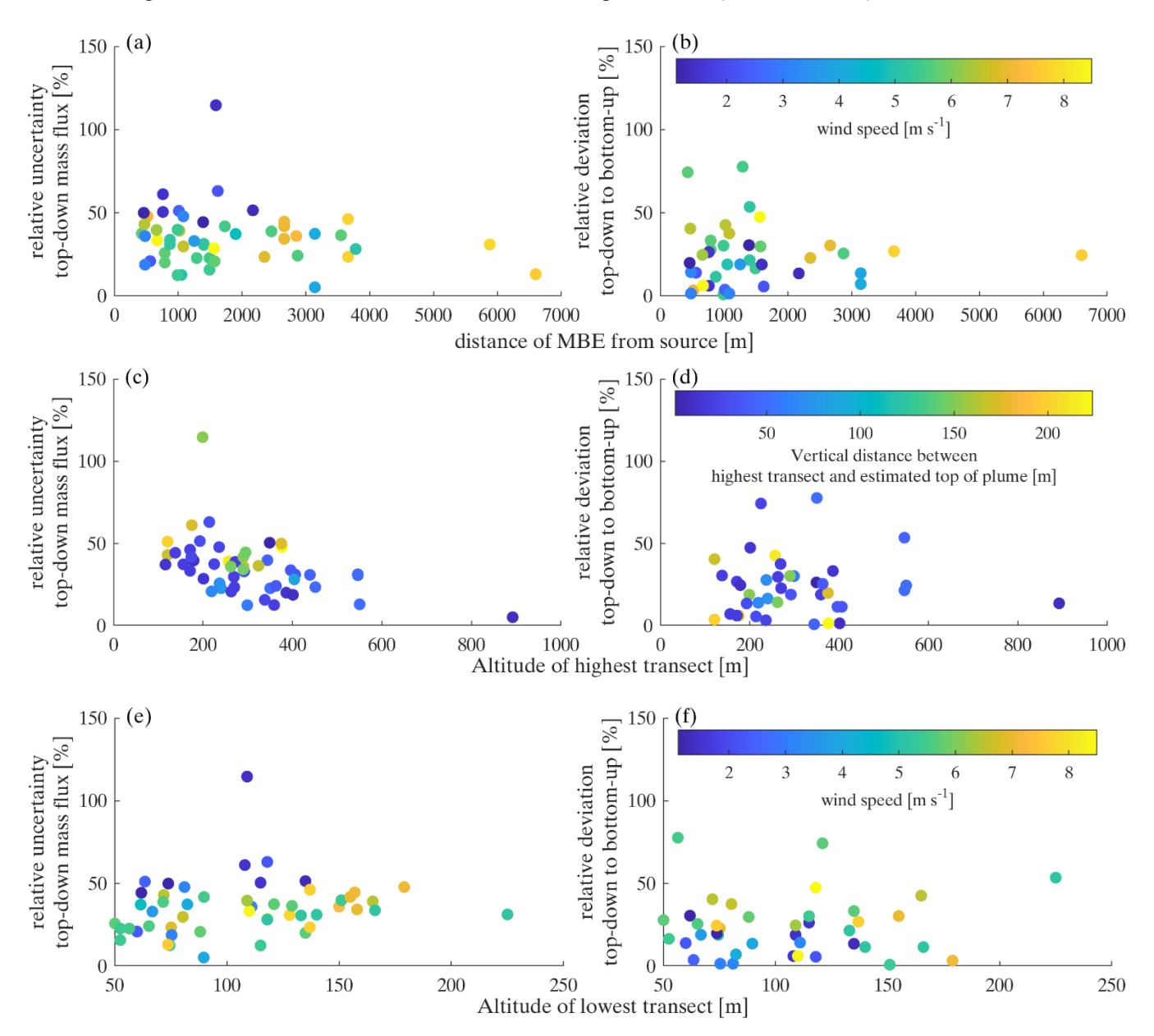


**Figure S11.** Relative mass flux uncertainty (**left**) and relative deviation of top-down and bottom-up mass fluxes (**right**) in dependency of (a, b) the distance of the MBEs from the emission source, colour-coded with the average wind speed and (**c**, **d**) the altitude of the highest transect, colour-coded with the vertical distance to the estimated top of the plume and (**e**, **f**) the altitude of the lowest transect, colour-coded with the wind speed This analysis includes 51 MBEs of our four targeted ventilation shafts for the relative uncertainty and 40 MBEs for the relative deviation to the in-mine data, based on Picarro measurements.

MBEs were conducted with maximum transect altitudes ranging from 100 m to 900 m (Fig. 11c, d). The results indicate that when the highest transect is lower the associated uncertainty is higher (Fig. 11c). The reasons might be that the higher parts of the plume were missed or that the plume was probed too close to the source, where the vertical extent was still low. Due to our approach described in Sect. S4, where half of the mass flux estimate resulting from the layer of the highest transect to the top of the plume is added to the total uncertainty, larger vertical distances between the highest transect and the estimated top of

the plume can lead to a higher uncertainty. However, an impact on the relative deviation between the top-down and the bottomup estimates is not evident (Fig. S11d).

According to the vertical profile measurements during MTG-Poland, the top of the CH<sub>4</sub> plume was on average located at  $\sim$ 370 m, while the average top of the closest inversion layer was located slightly higher at  $\sim$ 490 m (see Table 3 in the main document). Thus, the plume was mostly probed before it reached the top of the closest inversion layer. Depending on the available time (in general  $\sim$ 1.0 hour to 1.5 hours on site),  $\sim$ 5 to 10 transects were flown evenly distributed over the estimated plume extent to assure a sufficiently dense coverage of the plume. Since every transect requires flight time, greater numbers of transects are not recommended for a MBE, as the meteorological situation and hence the plume behaviour may change during the probing time.

The altitude of the lowest probed transect ranged from 50 m to 225 m (Fig. S11e, f). The mass flux uncertainty tends to slightly increase with altitude of the lowest transect, as expected. However, higher uncertainties above 50 % occurred mostly during situations with low wind speed. For the lowest transect, the same approach as for the highest transect was applied, as described above (if no mobile ground-based measurements were available): Half of the mass flux estimate resulting from the layer of the lowest transect to the ground is added to the total uncertainty, since it is not certain that the plume reaches the ground.

# S5.3 Time of probing

Another question is if the time of probing, e.g. time of day or year (season), has an influence on the estimated mass fluxes. Figure S12a suggests that there might be higher relative uncertainties for flights with a take-off before 11:00 LT.

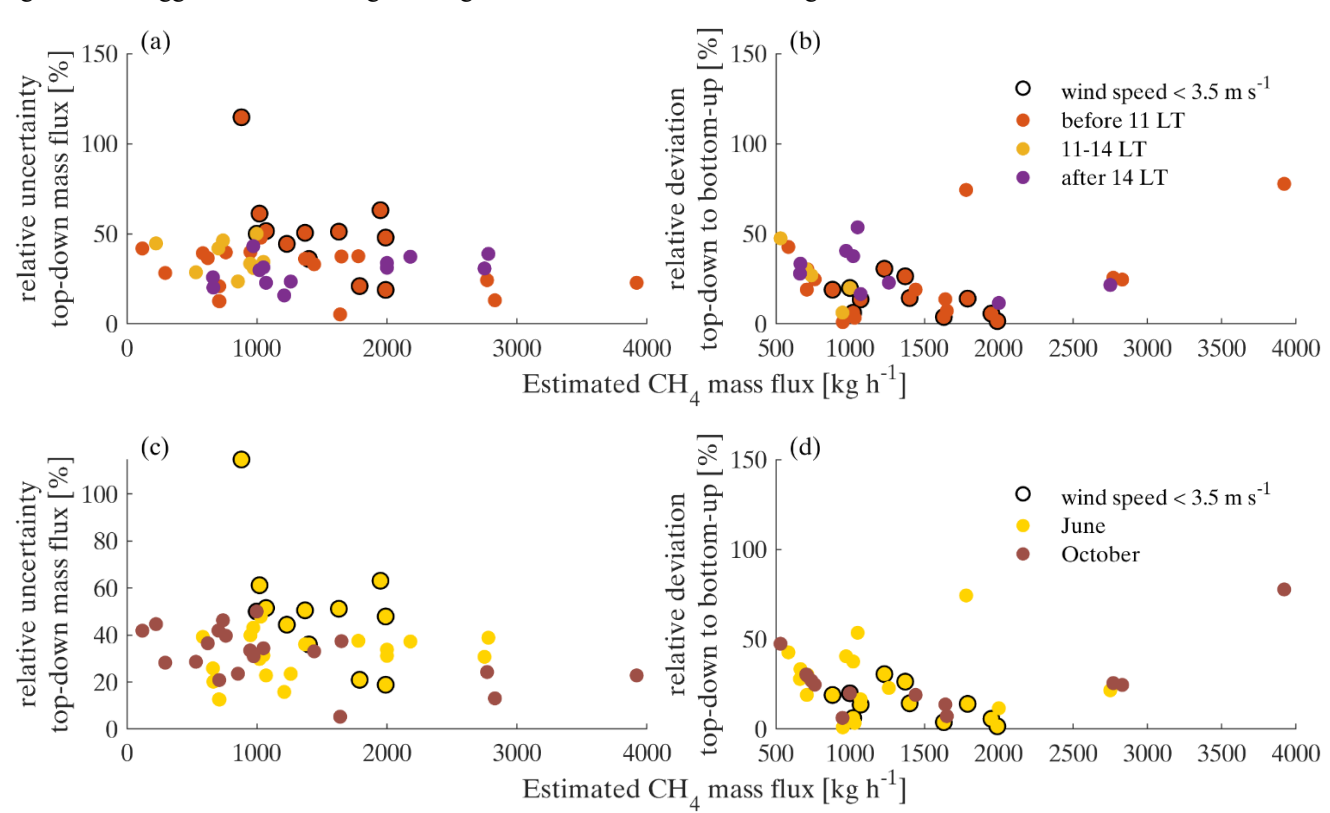


**Figure S12.** Relative mass flux uncertainty (**left**) and relative deviation of top-down and bottom-up mass fluxes (**right**) in dependency of the estimated top-down mass flux, colour-coded with (**a**, **b**) different spans for the take-off time and (**c**, **d**) with the month of the campaign. The flight time is usually 3 hours. MBEs with wind speeds smaller than 3.5 m s<sup>-1</sup> are marked by black circles. This analysis includes 51 MBEs of our four targeted ventilation shafts for the relative uncertainty and 40 MBEs for the relative deviation to the in-mine data, based on Picarro measurements.

However, as indicated by the black circles, the higher uncertainty is again caused by low wind speeds. Below a relative uncertainty of 50 %, there is no difference in uncertainties between different flight times. The same is true for the relative deviation of top-down estimates to the bottom-up data (Fig. S12b). The reason might be that due to the mostly complete vertical

coverage of the plume (several kilometres downwind of the source and within one hour) the development of the PBL may not have a strong influence on the mass flux uncertainty and accuracy of the estimated mass fluxes. The same point is valid when comparing the mass flux estimates of different seasons (Fig. S12c, d).

#### S6 Controlled CH<sub>4</sub> release

A controlled CH<sub>4</sub> release was conducted to validate our mass balance approach for emission detection and quantification (e.g. Morales et al., 2022). The release point was located in a corner in the southwestern part of the Bielsko-Biała airfield due to south-westerly wind directions on both days (Fig. S13a). Nearly perpendicular to the wind direction, the helicopter and *HELiPOD* could easily fly along the runway at different altitudes at a distance of ~330 m from the CH<sub>4</sub> release point. Mobile ground-based CH<sub>4</sub> measurements were performed by car north of the runway, as well as along the airport fence.

In summary, three controlled CH<sub>4</sub> releases were performed, two of them for the *HELiPOD* and one for a small drone. The latter set-up and results are described separately in Bretschneider et al. (2024). CH<sub>4</sub> was constantly released from three parallel operating 50 l gas bottles filled with 200 bar at the beginning (Air Liquide CH<sub>4</sub> 2.5 with a purity >99.5 %). The release rate was maintained with a Bronkhorst mass flow controller with a range of 0 to 1000 standard litre per minute (sl min<sup>-1</sup>) at ~500 sl min<sup>-1</sup> with an uncertainty of 10 sl min<sup>-1</sup> ( $\pm$  1 % reading plus  $\pm$  0.5 % full scale), corresponding to a mass flux uncertainty of ~0.5 kg h<sup>-1</sup> (500 sl min<sup>-1</sup> \* 0.00072 kg sl<sup>-1</sup> \* 60 min h<sup>-1</sup>). Due to this high flow, the quick pressure loss in the bottles lead to a strong cooling of the gas. To prevent the tubes from freezing, they were put into a water tub. The bottles were balanced with a scale before and after each release to determine the loss of weight. The uncertainty of the weighing is estimated to be ~0.3 kg. In order to release CH<sub>4</sub> several meters above the ground, an extendible mast with a height of 7.2 m above ground was used (Fig. S13b).

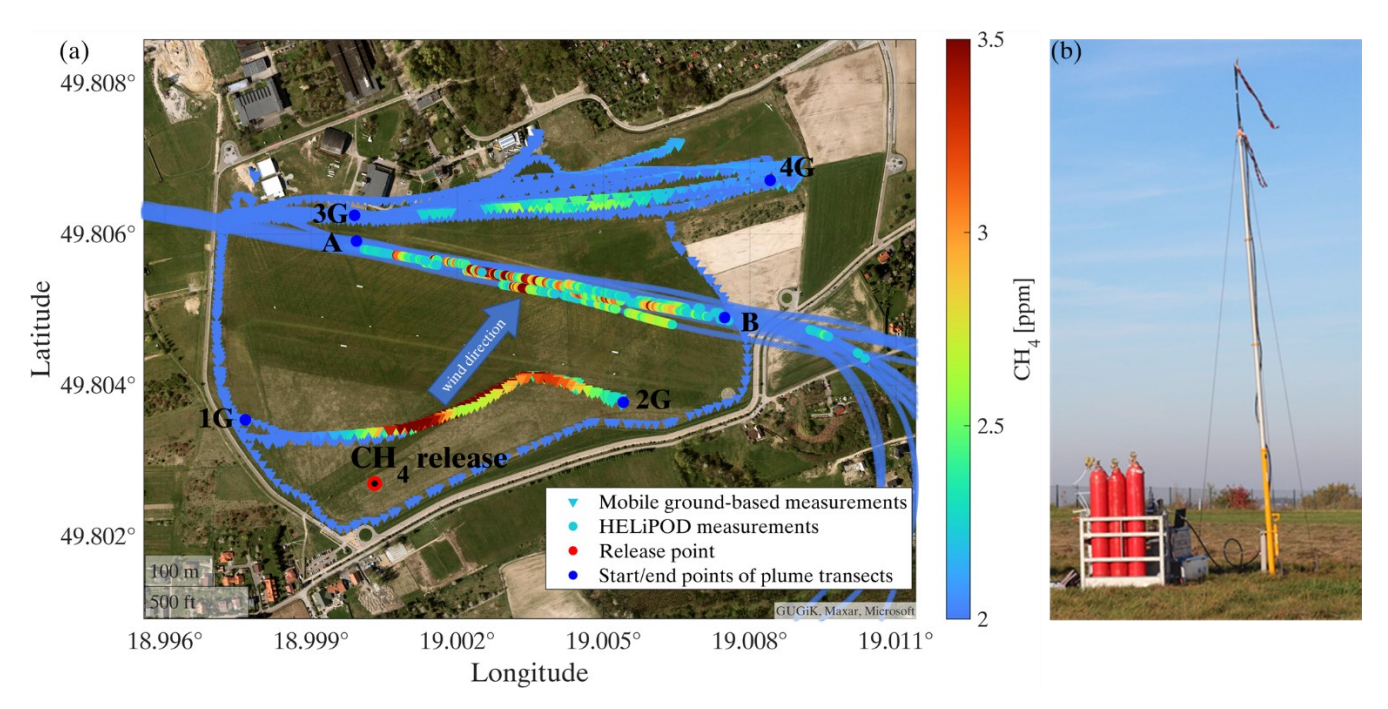


**Figure S13.** (a) Shown are the selected CH<sub>4</sub> release point on 17 and 18 October in the southwestern corner of the Bielsko-Biala airfield and the prevailing wind direction. Almost parallel to the main runway, the helicopter with the *HELiPOD* flew ~14 downwind transects at different vertical levels (CH<sub>4</sub> measurements shown for release #1 on 17 October 2022) between points A and B at a distance of ~330 m from the CH<sub>4</sub> release point. Mobile ground-based CH<sub>4</sub> measurements were performed between points 1G and 2G, 3G and 4G, as well as along the airport fence. (b) Release point of the CH<sub>4</sub> at an altitude of 7.2 m from three gas bottles. Photo courtesy by Sven Bollmann.

Figure S13a shows the transects of the *HELiPOD* and of the mobile ground-based measurements colour-coded with CH<sub>4</sub> concentrations during Release #1 on 17 October and verifies that the plume was successfully captured. The wind conditions were optimal for the probing with a wind speed of ~5 m s<sup>-1</sup> and a constant wind direction from ~200°. The lowest transect of

the *HELiPOD* was performed at an altitude of 5 m above ground, the plume height was approximately 35 m. The plume was penetrated right after take-off and  $\Delta$ CH<sub>4</sub> up to 1.5 ppm was observed downwind of the release point. The total released amount of CH<sub>4</sub> was 20.06 kg in 56.8 min, corresponding to 21.2 kg h<sup>-1</sup> ± 0.5 kg h<sup>-1</sup> (Release 1) and 14.61 kg in 41.2 min, corresponding to 21.3 kg h<sup>-1</sup> ± 0.5 kg h<sup>-1</sup> (Release 2).

From the vertical profiles in Fig. S14, it is evident that no pronounced inversion layers were present within the first 100 m, which might have impacted the vertical plume spreading. The top of the plume was approximately at an altitude of 35 m during Release 1 and 60 m during Release 2 (Fig. 12 and Fig. S14c). The mean plume width was ~120 m and ~63 m, respectively. The reason for the narrower and higher located plume during Release 2 is most likely related to the different stratification of the lowest 100 m. During Release 2, the potential temperature profile in Fig. S14b indicates a more unstable stratification (slightly decreasing temperature with altitude) compared to Release 1 (slightly increasing temperature with altitude). During Release 1, the weather situation was impacted by foehn winds over the Western Beskids, which caused this more stable stratification of the lowest 100 m. On both days, the plume was probed by 12 to 14 *HELiPOD* transects and 5 to 10 mobile ground-based transects.

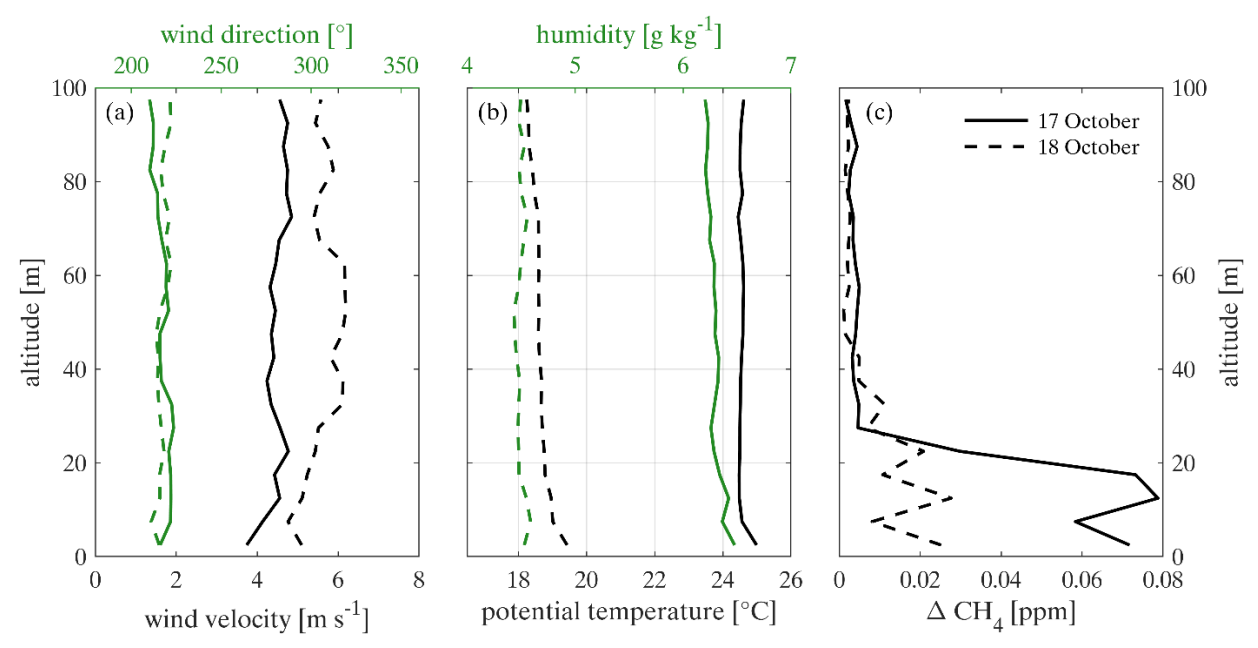


**Figure S14.** Mean profiles of (a) wind direction and velocity, (b) humidity and potential temperature, and (c) CH<sub>4</sub> enhancement over background for altitude bins of 5 m during the controlled CH<sub>4</sub> releases in October 2022.

As described in the main document, the flight altitude changes during the plume crossing with multiple overlaying transects (Fig. 12 in the main document). In this case, the method introduced in Sect. 2.3 and Sect. 2.4 of the main document (Approach 1) might not result in correct mass flux estimates, when applied in the same way. Therefore, we used two additional approaches to estimate the mass flux during the release experiment. For Approach 2, we average the measured parameters of Eq. 2 for an altitude bin of 5 m (Release 1) and 10 m (Release 2) and calculate the mass flux for every bin. The total mass flux is then the sum of the bins. The uncertainty is estimated by using only every second, third and fourth transect for bin averaging. The uncertainty is then the standard deviation of these mass flux estimates. For Approach 3, we use a common single-transect approach known from the literature (Cambaliza et al., 2014; Fiehn et al., 2020). Since the vertical plume extent is small and more than 10 transects were performed to statistically cover the changing dynamic behaviour of the plume, we assume that the average of separately calculated mass fluxes of multiple single transects should yield an approximate mass flux estimate for the release rate. The mass flux uncertainty is the standard deviation of all single transect mass flux estimates. For each of the three approaches, we consider only mobile ground-based transects which fully crossed the plume. We calculate the CH<sub>4</sub> enhancement by subtracting a mean CH<sub>4</sub> background concentration at an altitude between 0 m to 100 m from the edges of the plume, for each release day separately.

As expected, estimates with Approach 1 are too small (-31 %), because the calculated heights of the transects were probably imprecise due to the overlaying transects and changing altitudes during crossing. The binning of Approach 2 shows a good agreement to the released amount for Release 1 (deviation of 3 %) but the same large deviation for Release 2 (-33 %) as for Approach 1. Here, using less overlaying transect might result in comparable results of Approach 1 and 2. The single-transect Approach 3 shows good agreement for Release 1 and 2 (deviation of -2 and -8 % to the released amount, respectively) but, as expected, has much higher uncertainties of 55 % and 70 %, respectively, due to the large variability of the single-transect estimates. However, this uncertainty range is comparable to the single-transect approach of Cambaliza et al. (2014).

The estimated release rates for the combination of airborne and ground-based transects agree well with the actual release rate of ~21 kg h<sup>-1</sup>, showing a relative uncertainty ranging from 13 % to 70 % (Table S5) when mobile ground-based measurements are included, which is comparable to Cambaliza et al. (2014). When the ground-based data are excluded, estimates for Release #1 are nearly the same, whereas for Release #2 the estimates are lower (~13 kg h<sup>-1</sup> to 15 kg h<sup>-1</sup>). An explanation for the observed decrease could be that the plume was less mixed in this first 50 m above ground due to slightly higher wind speeds (5.8 m s<sup>-1</sup> versus 4.1 m s<sup>-1</sup>) in the latter case. If the plume "core", which contains the highest concentrations, predominately stays close to the ground due to higher wind speeds, ground-based measurements may help to increase the accuracy, as shown in Table S5 for Release 2.

**Table S5.** Estimated CH<sub>4</sub> release rates for three approaches of the controlled CH<sub>4</sub> releases on 17 and 18 October 2022, calculated for 2 Hz Picarro measurements, as well as in- and excluding mobile ground-based measurements. The distance of the measurements to the release point is  $\sim$ 330 m. The actual CH<sub>4</sub> release rate is 21.2 kg h<sup>-1</sup> on 17 October and 21.3 kg h<sup>-1</sup> on 18 October. The uncertainty is given as the relative standard deviation of all single-transect mass fluxes.

			With n	nobile ground-	based	Without	mobile ground	d-based
Release date	Released	Approach	Estimated	Uncertainty	Deviation	Estimated	Uncertainty	Deviation
in 2022	[kg h <sup>-1</sup> ]		[kg h <sup>-1</sup> ]	[%]	[%]	[kg h <sup>-1</sup> ]	[%]	[%]
17.0 . 1		1	$14.7 \pm 1.9$	13	-31	$14.1 \pm 1.6$	11	-33
17 October, 12:37–13:34 LT	$\textbf{21.2} \pm 0.5$	2	$21.5 \pm 6.3$	29	1	$21.7 \pm 6.4$	29	2
12.57-15.54 L1		3	$20.7 \pm 11.4$	55	-2	$20.7 \pm 12.5$	60	-3
10.0 . 1		1	$14.6 \pm 2.5$	17	-31	$14.2 \pm 3.5$	25	-33
18 October, 09:37–10:18 LT	$\textbf{21.3} \pm 0.5$	2	$13.9 \pm 2.4$	17	-34	$13.6 \pm 2.7$	20	-36
09.57-10.16 L1		3	$19.6 \pm 13.8$	70	-8	$14.8 \pm 9.0$	61	-31

To improve the quality of the mass flux estimates for future controlled release experiments with the *HELiPOD*, we recommend i) to keep the flight altitudes of the transects as constant as possible, ii) to conduct the MBE with less transects and defined altitudes in a fixed interval from the lower to the upper plume limit (for the present set-up at a distance of  $\sim$ 300 m, intervals of  $\sim$ 5 m to 10 m would be appropriate) and iii) to use e.g. inverse modelling to assess the plume dispersion of the anticipated release rates in the target area of the experiment and plan the probing distances and intervals according to the modelling results.

# S7 Overview of calculated CH<sub>4</sub> mass fluxes

**Table S6.** Calculated CH4 mass flux rates with uncertainties from the shaft **Knurów-Szczyglowice IV** (Shaft 1), June 2022 and comparison to bottom-up in-mine estimates. D – distance of MBE to shaft, FF – wind speed, DD – wind direction,  $\emptyset$  - average for all plumes of the MBE,  $\sigma$  - root-mean-square error, Top – plume height, A TS1 – altitude of lowest transect, GB – ground-based transects included (yes/no), R – time resolution of data. Comment explanation: "Earlier TSs" (transects): probing closer to take-off, "later TSs": probing closer to landing. DRAINAGE STATION: mass flux estimates of nearby drainage station. The bold values of the *HELiPOD* mass fluxes are used to calculate the mean mass flux per flight listed in Table 4 in the main document. For details to the flight date and time, see Table S1.

										maximum	time				HELI	POD	In-min	e data	relative	
	D	tra	nsects	FF [r	n s <sup>-1</sup> ]	DD	[°]	Top	A TS1	since take-o	off [h]	GB		R	flux	unc.	flux	unc.	deviation	
flight	[m]	flown	selected	Ø	σ	Ø	σ	[m]	[m]	HELIPOD	GB	included	Instr.	[Hz]	[kg	h <sup>-1</sup> ]	[kg	h <sup>-1</sup> ]	[%]	comment
F03	1050	7	4	4.0	1 2	205	10	200	76	1.2			Picarro	2	841	83	874	20	-4	
FU3	1050	/	4	4.8	1.2	285	19	380	76	1.3		no	Licor	40	803	100	874	30	-8	
				4.6	17	302	10	400	129	1.3			Picarro	2	665	134	998	27	-33	Earlier TSs
F04	790	24	6	4.0	1.7	302	18	400	129	1.5		no	Licor	40	637	134	998	21	-36	Earlier 138
FU4	790	24	10	5.7	1.3	306	15	309	48	2.9			Picarro	2	662	171	918	18	-28	Later TSs
		<u> </u>	10	J./	1.5	300	15	309	40	2.9		no	Licor	40	608	158	210	19	-34	Later 135

	1490	13	5	5.3	1.4	312	16	313	53	2.9		no	<b>Picarro</b> Licor	<b>2</b> 40	1030	<b>244</b> 286	918	18	17 12	
	1490	13	10	5.3	1.4	312	16	313	53	2.9		no	Picarro Licor	2 40	1210 1210	191 236				DRAINAGE STATION 1
	760	10	4	1.5	0.8	40	93	350	108	1.1		no	Picarro Licor	<b>2</b> 40	<b>1370</b> 1350	<b>692</b> 636	1084	32	26 25	Earlier TSs
F05	760	10	4	1.5	0.8	40	93	350	104	1.5		no	Picarro Licor	<b>2</b> 40	<b>1020</b> 987	<b>624</b> 633	1087	23	-6 -9	Later TSs
	1590	3	3	1.3	0.8	122	88	350	108	0.4		no	Picarro Licor	<b>2</b> 40	<b>881</b> 700	<b>1010</b> 870	1087	23	-19 -36	
												no	Picarro Licor	2	1030 959	493 464	996	41	3 -4	
	520	7	2	7.1	1.4	223	10	340	171	1.7	2.1	yes	Picarro Licor	<b>2</b>	<b>1020</b> 965	<b>170</b> 177	996	41	2 -3	
F06		_	_									no	Picarro Licor	2 40	584 747	229 360	1019	40	-43 -27	
	1020	8	7	6.4	1.5	220	13	470	167	2.2	2.1	yes	Picarro Licor	<b>2</b> 40	<b>961</b> 948	<b>397</b> 356	1019	40	-6 -7	
	2850	7	5	7.1	1.6	228	10	470	148	2.3		no	Picarro Licor	2 40	1370 1340	494 601	967	24	42 39	DRAINAGE
		_										no	Picarro Licor	2 40	1780 1710	668 680	1021	28	74 67	
	430	6	3	5.7	1.4	213	14	251	119	1.8	2.1	yes	Picarro Licor	<b>2</b> 40	<b>1310</b> 1270	<b>187</b> 230	1021	28	28 24	
			_									no	Picarro Licor	2 40	950 964	379 421	941	27	1 2	
507	000	10	4	5.3	1.3	217	14	386	152	1.0	2.1	yes	<b>Picarro</b> Licor	<b>2</b> 40	<b>868</b> 884	<b>126</b> 162	976	48	-11 -9	
F07	990	10	5	г э	1 2	217	14	252	115	2.4		no	Picarro Licor	2 40	712 699	89 150	1021	28	-30 -32	
		10	5	5.3	1.3	217	14	352	115	2.1	2.1	yes	<b>Picarro</b> Licor	<b>2</b> 40	<b>840</b> 829	<b>92</b> 148	1021	28	-18 -19	
	2056	40	5	5.6	1.2	213	13	500	159	1.2		no	Picarro Licor	2 40	2350 2340	809 1050	941	27	150 149	Mixed with drainage
	2850	10	5	5.6	1.2	213	13	378	137	2.1		no	Picarro Licor	2 40	2700 2720	1300 1400	1021	28	164 166	Mixed with drainage

**Table S7.** Calculated CH<sub>4</sub> mass flux rates with uncertainties from the shaft **Brzeszcze-Andrzej IX** (Shaft 2), June 2022. For abbreviations see Table S6. During F12, the GB data does not fit to the early TS, because the coal mine company changed the flux from 1634 kg  $h^{-1}$  to 1960 kg  $h^{-1}$  before the GB data was measured.

	D		nsects		m s <sup>-1</sup> ]	DD		Тор		maximum since take-c	off [h]	GB		R	HELi flux	unc.	In-min flux	unc.	relative deviation	
flight	[m]	flown	selected	Ø	σ	Ø	σ	[m]	[m]	HELIPOD	GB	included	Instr.	[Hz]	[kg		[kg	h-1]	[%]	comment
			7	6.0	1.2	240	17	336	162	0.4		no	Picarro	2	2000	676	2262	452	-12	Earlier TSs
	870	14											Licor	40	1980	735	•		-12	
			4	6.0	1.2	240	17	435	141	1.7		no	Picarro	2	2000	623	2262	452	-12	Later TSs
									•	-			Licor	40	1970	661	•		-13	
F08			10	5.2	1.1	241	15	599	133	2.0		no	Picarro		2720	845 899	2262	452	20	All TS
							•						Licor Picarro	40 <b>2</b>	2640 <b>1050</b>	329	•		17 - <b>54</b>	
	1400	12		5.2	1.1	241	14	589	225	1.3		no	Licor	40	997	384	2262	452	-5 <del>4</del> -56	Earlier TSs
			6				•						Picarro		2750	845	•		22	
				5.2	1.1	241	15	599	133	2.0		no	Licor	40	2650	896	2262	452	17	Later TSs
													Picarro	2	972	419			-41	
				7.0	1.3	304	9.2	290	72	1.6		no	Licor	40	927	414	1634	327	-43	
	470	8	4						•			•••••	Picarro	2	1460	363	•		-11	
				7.0	1.3	304	9.2	290	72	1.6	1.1	yes	Licor	40	1420	368	1634	327	-13	
													Picarro	2	1020	304			-38	
			_	6.7	2.0	297	8.9	290	80	2.7		no	Licor	40	980	312	1634	327	-40	
	1080	9	7	<i>c</i> -		207		200		2.7	4 7		Picarro	2	1520	324			-7	
F10				6.7	2.0	297	8.9	290	80	2.7	1.7	yes	Licor	40	1490	336	1634	327	-9	
F10				7.0	1.7	297	10	290	75	1.8			Picarro	2	1260	296	1634	327	-23	
	2350	9	9	7.0	1.7	297	10	290	/5	1.8		no	Licor	40	1220	365	1034	327	-25	
	2330	9	9	7.0	1.7	297	10	290	75	1.8	1.3	voc	Picarro	2	1460	176	1634	327	-11	
				7.0	1.7	297	10	290	75	1.0	1.5	yes	Licor	40	1440	242	1034	327	-12	
	1900	13	11	5.0	1.5	296	10	130	63	2.4		no	Picarro	2	2180	812				DRAINAGE
	1300	13		5.0	1.5	230		130		2.7		110	Licor	40	1780	743				STATION 2
	2460	13	11	5.7	1.7	297	13	290	72	2.5		no	Picarro	2	2780	1080				DRAINAGE
													Licor	40	2730	1350				STATION 2
				3.2	1.2	324	28	410	110	1.0		no	Picarro	2	1400	504	1634	327	-14	Earlier TSs
			4										Licor	40	1380	529			-16	
				3.2	1.2	324	28	410	110	1.0	1.6	yes	Picarro	2	1400	485				GB time
	480	15										·	Licor	40	1390	480	•			not fitting
F12				3.2	1.2	324	28	410	76	2.7		no	Picarro	2	1990	375	1960	392	2	
			11							•			Licor	40	1750	357			-11	
				3.1	1.1	323	29	410	76	2.7	1.6	yes	Picarro	2	2050	390	1960	392	5	Later TSs
										•			Licor	40	1850 <b>1990</b>	413	•		-6 2	
	1080	12	8	3.3	1.2	324	30	600	81	2.8		no	Picarro	<b>2</b>		<b>953</b> 1060	1960	392	5	
	l												Licor	40	2060	TOPO			5	

Table S8. Calculated CH<sub>4</sub> mass flux rates with uncertainties from the shaft Brzeszcze-Andrzej IX (Shaft 2), October 2022. For abbreviations see Table S6.

										maximum	time				HELi	POD	In-min	e data	relative	
	D	tra	nsects	FF [r	m s <sup>-1</sup> ]	DD	[°]	Top	A TS1	since take-o	ff [h]	GB		R	flux	unc.	flux	unc.	deviation	
flight	[m]	flown	selected	Ø	σ	Ø	σ	[m]	[m]	HELIPOD	GB	included	Instr.	[Hz]	[kg	h <sup>-1</sup> ]	[kg	h <sup>-1</sup> ]	[%]	comment
F04	460		7	1.1	0.7	250	0.4		60	1.0			Picarro	2	998	499	1246	240	-20	
F04	460	9	/	1.1	0.7	359	84	550	69	1.0		no	Licor	40	945	523	1246	249	-24	

**Table S9.** Calculated CH<sub>4</sub> mass flux rates with uncertainties from the shaft **Pniówek V** (Shaft 3), June 2022. For abbreviations see Table S6. Due to the low wind speed during flight F13, emission accumulation from the night inversion layer might be still present close to the emitter.

										maximum 1	time				HELi	POD	In-mir	ie data	relative	
	D	tra	nsects	FF [r	n s <sup>-1</sup> ]	DD	[°]	Top	A TS1	since take-o	ff [h]	GB		R	flux	unc.	flux	unc.	deviation	
flight	[m]	flown	selected	Ø	σ	Ø	σ	[m]	[m]	HELIPOD	GB	included	Instr.	[Hz]	[kg	h-1]	[kg	h-1]	[%]	comment
	560	8	5	2.3	0.8	222	58	283	61	1.8			Picarro	2	1790	375	1570	314	14	
	300	٥	5	2.3	0.8	222	20	203	91	1.8		no	Licor	40	1740	398	15/0	314	11	
			9	2.8	1.1	220	42	341	57	2.1		no	Picarro	2	4660	526	1740	348	168	Mixing with
			9	2.0	1.1	220	42	341	31	2.1		110	Licor	40	4170	605	1740	340	140	drainage
	1010	9	3	2.5	1.1	220	47	353	150	0.8		no	Picarro	2	5480	2220	1916	383	186	Mixing with
F09	1010	9	3	2.5	1.1		4/	333	130	0.8		110	Licor	40	4720	2140	1910		146	drainage
103			3	2.5	1.1	220	47	320	64	1.9		no	Picarro	2	1630	834	1570	314	4	
			3	2.3	1.1	220	4/	320		1.9		110	Licor	40	1730	911	1370	314	10	
			8	2.2	0.9	226	53	331	57	1.7		no	Picarro	2	4230	1750	1845	369	129	Mixing with
	1620	8	0	2.2	0.5			331		1./		110	Licor	40	3980	1520	1043		116	drainage
	1020	0	3	2.2	0.9	226	53	244	118	1.3		no	Picarro	2	1950	1230	1845	369	6	
			3	2.2	0.9	220	33	244	110	1.5		110	Licor	40	1920	1160	1043	309	4	
	600	12	6	1.1	0.5	99	58	241	55	2.7		no	Picarro	2	2040	945	942	188.4	117	Accumulation
	000	12		1.1	0.5			241		2./		110	Licor	40	2040	974	J4Z	100.4	117	Accumulation
F13	1390	7	5	1.1	0.6	84	56	158	62	2.7		no	Picarro	2	1230	546	942	188	31	
113	1330	,		1.1	0.0	04	30	130		2./		110	Licor	40	1200	531	342	100	27	
	2170	5	2	1.3	0.6	79	40	222	134	2.6		no	Picarro	2	1070	551	942	188	14	
	21/0	,	2	1.3	0.0	, 3	70	222	134	2.0		110	Licor	40	1050	560	J-42	100	11	

Table S10. Calculated CH<sub>4</sub> mass flux rates with uncertainties from the shaft Pniowek V (Shaft 3), October 2022. For abbreviations see Table S6.

										maximum	time				HELi	POD	In-min	e data	relative	
	D	tra	nsects	FF [r	n s <sup>-1</sup> ]	DE	) [°]	Top	A TS1	since take-o	off [h]	GB		R	flux	unc.	flux	unc.	deviation	
flight	[m]	flown	selected	Ø	σ	Ø	σ	[m]	[m]	HELIPOD	GB	included	Instr.	[Hz]	[kg	h <sup>-1</sup> ]	[kg	h <sup>-1</sup> ]	[%]	comment
												no	Picarro	2	1440	476	1778	356	-19	
	1250	10	7	3.7	1.1	74	14.0	329	64.6	1.3		110	Licor	40	1400	482	1//6	330	-21	
	1230	10	,	3.7	1.1	74	14.0	329	04.0	1.5	2.9	ves	Picarro	2	1820	427	1881	376	-3	
			-								2.9	yes	Licor	40	1760	441	1001	3/0	-6	
F03			5	4.1	0.8	80	15.0	180	82.4	1.2		no	Picarro	2	1650	617	1778	356	-7	Earlier TSs
103	3140	20	J	4.1			13.0	100	02.4	1.2		110	Licor	40	1640	660	1776	330	-8	Lamer 133
	3140	20	9	4.0	0.9	76	14.0	900	90.2	2.8			Picarro	2	1640	86	1900	380	-14	Later TSs
							14.0			2.0		no	Licor	40	1730	246			-9	
	6140	10	9	4.7	0.8	73	14.0	900	74.9	2.8		no	Picarro	2	4040	493	1985	397	103	Mixing with
	0140	10	9	4.7	0.8	73	14.0	300	74.5	2.6		110	Licor	40	3840	815	1965	337	93	drainage
												no	Picarro	2	3920	894	2206	441	78	
	1290	11	8	5.5	3.2	229	11.0	400	56.3	1.7		110	Licor	40	3810	977	2200		73	
	1230		o	5.5	3.2	223	11.0	400	30.3	1.7	3.0	ves	Picarro	2	3400	373	2244	449	52	
F05											3.0	yc3	Licor	40	3300	455			47	
103	2870	10	8	5.7	2.9	232	9.6	400	63.1	1.7		no	Picarro	2	2770	672	2206	441	26	
	2070	10		J./	2.3		3.0	400		1./		110	Licor	40	2780	793			26	
	6600	9	8	7.5	1.4	232	8.3	600	73.7	2.8		no	Picarro	2	2830	370	2272	454	25	
	0000	3		,.5	1.4	232	0.3	000	, 3.7	2.0		110	Licor	40	2720	581	22/2	734	20	

Table S11. Calculated CH<sub>4</sub> flux rates with uncertainties from the shaft Agnieszka-Powietrzny V (Shaft 4), October 2022. For abbreviations see Table S6. SHAFT 5 is Erbreich-Powietrzny I.

										maximum	time				HELil	POD	In-min	e data	relative	
	D		nsects		n s <sup>-1</sup> ]		) [°]		A TS1	since take-o		GB		R	flux	unc.	flux	unc.	deviation	
flight	[m]	flown	selected	Ø	σ	Ø	σ	[m]	[m]	HELIPOD	GB	included	Instr.	[Hz]	[kg		[kg	h <sup>-1</sup> ]	[%]	comment
												no	Picarro	2	948	317	1011	470	-6	
	670	5	3	8.7	1.6	212	6.1	185	115	1.3			Licor	40	837	311			-17	
	0,0		J	0.,	2.0		0.1	100	113	2.0	1.7	yes	Picarro	2	1040	156	1011	470	3	
			•						•	•			Licor	40	980	168			-3	
												no	Picarro	2	531	152	1011	470	-47	
	1560	7	4	8.5	2.0	213	8.2	214	117	1.4			Licor	40	506	179	•		-50	
											1.7	yes	Picarro	2	829	172	1011	470	-18	
			•••••						•	•	<u> </u>		Licor	40	800	192	•		-21	
	2660	3	3	7.0	1.4	210	8.7	440	157	0.2		no	Picarro	2	704	295	1011	470	-30	
F06													Licor	40	717	384			-29	
	3660	6	2	7.7	1.3	221	7.6	191	137	1.8		no	Picarro	2	<b>739</b> 769	<b>342</b> 421	1011	470	-27	
													Licor	40	1050	361			-24	
	2660	3	3	7.0	1.6	212	8.6	440	157	0.2		no	Picarro Licor	40	961	349				SHAFT 5
			•				•		•	•			Picarro	2	854	201	•			
	3660	6	6	7.7	1.4	220	8.1	500	137	0.7		no	Licor	40	815	291				SHAFT 5
			•••••				•	••••••	•	•	•	<b></b>	Picarro	2	975	302	•		·····	
	5880	6	6	7.8	1.1	218	8.0	481	129	0.7		no	Licor	40	1050	508				SHAFT 5
													Picarro	2	224	100				DRAINAGE
	2660	3	3	7.1	1.6	210	9.2	440	156	0.2		no	Licor	40	223	130				STATION 4
													Picarro	2	761	302			-25	
		_										no	Licor	40	746	329	1011	470	-26	
	660	7	4	5.9	1.2	212	8.3	193	106	1.5			Picarro	2	900	249			-11	
											3.9	yes	Licor	40	877	259	1011	470	-13	
									•				Picarro	2	710	140	1011	470	-30	
	1570	9	8	Е 0	1 /	211	11.0	201	90.5	1.7		no	Licor	40	704	196	1011	470	-30	
	1370	9	0	5.6	1.4	211	11.0	204	90.5	1.7	3.9	VOC	Picarro	2	861	181	1011	470	-15	
F07											3.9	yes	Licor	40	858	225	1011	470	-15	
107	3550	6	5	5.4	1 /	210	10.0	490	129	2.4		no	Picarro	2	398	75	1011	470	-61	Mixed with
	3330	ŭ		J. <del>-</del>	1.4	210	10.0	730	123	2.7		110	Licor	40	390	162	1011	470	-61	SHAFT 5
		9	6	5.4	1 3	211	11.0	200	89.6	1.4		no	Picarro	2	119	50				DRAINAGE
	3550			J.¬						±T			Licor	40	90	37	•			STATION 4
	3330	6	5	49	1.3	207	11.0	490	117	2.4		no	Picarro	2	295	83				DRAINAGE
			-										Licor	40	329	246				STATION 4
	3550	6	4	5.4	1.4	210	10.0	490	129	2.3		no	Picarro	2	622	227				SHAFT 5
				- '						-			Licor	40	604	287				

## References

Bretschneider, L., Bollmann, S. B., Houssin-Agbomson, D., Shaw, J., Howes, N., Nguyen, L., Robinson, R., Helmore, J., Lichtenstern, M., Nwaboh, J., Pogány, A., Ebert, V., and Lampert, A.: Concepts for Drone Based Pipeline Leak Detection, Front. Robot. AI, 11, https://doi.org/10.3389/frobt.2024.1426206, 2024.

Cambaliza, M. O. L., Shepson, P. B., Caulton, D. R., Stirm, B., Samarov, D., Gurney, K. R., Turnbull, J., Davis, K. J., Possolo, A., Karion, A., Sweeney, C., Moser, B., Hendricks, A., Lauvaux, T., Mays, K., Whetstone, J., Huang, J., Razlivanov, I., Miles, N. L., and Richardson, S. J.: Assessment of uncertainties of an aircraft-based mass balance approach for quantifying urban greenhouse gas emissions, Atmos. Chem. Phys., 14, 9029–9050, https://doi.org/10.5194/acp-14-9029-2014, 2014.

Edie, R., Robertson, A. M., Field, R. A., Soltis, J., Snare, D. A., Zimmerle, D., Bell, C. S., Vaughn, T. L., and Murphy, S. M.: Constraining the accuracy of flux estimates using OTM 33A, Atmospheric Measurement Techniques, 13, 341–353, https://doi.org/10.5194/amt-13-341-2020, 2020.

Fiehn, A., Kostinek, J., Eckl, M., Klausner, T., Gałkowski, M., Chen, J., Gerbig, C., Röckmann, T., Maazallahi, H., Schmidt, M., Korbeń, P., Neçki, J., Jagoda, P., Wildmann, N., Mallaun, C., Bun, R., Nickl, A.-L., Jöckel, P., Fix, A., and Roiger, A.: Estimating CH<sub>4</sub>, CO<sub>2</sub> and CO emissions from coal mining and industrial activities in the Upper Silesian Coal Basin using an aircraft-based mass balance approach, Atmospheric Chemistry and Physics, 20, 12675–12695, https://doi.org/10.5194/acp-20-12675-2020, 2020.

Lampert, A., Pätzold, F., Asmussen, M. O., Lobitz, L., Krüger, T., Rausch, T., Sachs, T., Wille, C., Sotomayor Zakharov, D., Gaus, D., Bansmer, S., and Damm, E.: Studying boundary layer methane isotopy and vertical mixing processes at a rewetted peatland site using an unmanned aircraft system, Atmos. Meas. Tech., 13, 1937–1952, https://doi.org/10.5194/amt-13-1937-2020, 2020.

Mallaun, C., Giez, A., and Baumann, R.: Calibration of 3-D wind measurements on a single-engine research aircraft, Atmos. Meas. Tech., 8, 3177–3196, https://doi.org/10.5194/amt-8-3177-2015, 2015.

Morales, R., Ravelid, J., Vinkovic, K., Korbeń, P., Tuzson, B., Emmenegger, L., Chen, H., Schmidt, M., Humbel, S., and Brunner, D.: Controlled-release experiment to investigate uncertainties in UAV-based emission quantification for methane point sources, Atmospheric Measurement Techniques, 15, 2177–2198, https://doi.org/10.5194/amt-15-2177-2022, 2022.

Pätzold, F., Bretschneider, L., Nowak, S., Brandt, B., Schlerf, A., Asmussen, M. O., Bollmann, S., Bärfuss, K., Harm-Altstädter, B., Hecker, P., Wehner, B., van der Wall, B. G., Sachs, T., Huntrieser, H., Roiger, A., and Lampert, A.: HELiPOD—Revolution and evolution of a helicopter-borne measurement system for multidisciplinary research in demanding environments, Elementa: Science of the Anthropocene, 11, 00031, https://doi.org/10.1525/elementa.2023.00031, 2023.

Pühl, M., Roiger, A., Fiehn, A., Gorchov Negron, A. M., Kort, E. A., Schwietzke, S., Pisso, I., Foulds, A., Lee, J., France, J. L., Jones, A. E., Lowry, D., Fisher, R. E., Huang, L., Shaw, J., Bateson, P., Andrews, S., Young, S., Dominutti, P., Lachlan-Cope, T., Weiss, A., and Allen, G.: Aircraft-based mass balance estimate of methane emissions from offshore gas facilities in the southern North Sea, Atmospheric Chemistry and Physics, 24, 1005–1024, https://doi.org/10.5194/acp-24-1005-2024, 2024.